# RBM39 shapes innate immunity through transcriptional and splicing control of IRF3 and other key factors

**Authors:** Teng-Feng Li[1], Arthur Lang[1], Paul Rothhaar[1], Oliver Grünvogel[1], Ombretta Colasanti[1], Santa Mariela Olivera Ugarte[1], Jannik Traut[1], Antonio Piras[2], Nelson Acosta-Rivero[3], Vladimir Gonçalves Magalhães[4], Emely Springer[5], Andreas Betz[1], Hao-En Huang[1], Jeongbin Park[6], Ruiyue Qiu[7], Gnimah Eva Gnouamozi[3], Ann-Kathrin Mehnert[8], Viet Loan Dao Thi[8,9], Stephan Urban[3,9], Martina Muckenthaler[7], Matthias Schlesner[6,10], Dirk Wohlleber[5], Marco Binder[4], Ralf Bartenschlager[3,4,9], Andreas Pichlmair[2,11], Volker Lohmann[1,9]*

**Affiliations:**

[1] Department of Infectious Diseases, Molecular Virology, Section Virus-Host-Interactions, Medical Faculty Heidelberg, Heidelberg University, Heidelberg, Germany.

[2] Institute of Virology, School of Medicine, Technical University of Munich, Munich, Germany.

[3] Department of Infectious Diseases, Molecular Virology, Medical Faculty Heidelberg, Heidelberg University, Heidelberg, Germany.

[4] Division of Virus-Associated Carcinogenesis, German Cancer Research Center (DKFZ), Heidelberg, Germany.

[5] Institute of Molecular Immunology, University Hospital Klinikum rechts der Isar, Technical University of Munich, Munich, Germany.

[6] Bioinformatics and Omics Data Analysis, German Cancer Research Center (DKFZ), Heidelberg, Germany.

[7] Heidelberg University, Medical Faculty, Department of Pediatric Oncology, Hematology, Immunology and Pneumology, Heidelberg, Germany.

[8] Department of Infectious Diseases, Virology, Medical Faculty Heidelberg, Heidelberg University, Heidelberg, Germany.

[9] German Center for Infection Research (DZIF), Heidelberg Partner Site, Heidelberg, Germany.

[10] Biomedical Informatics, Data Mining and Data Analytics, Faculty of Applied Computer Science and Medical Faculty, University of Augsburg, Augsburg, Germany

[11] German Center for Infection Research (DZIF), Munich Partner Site, Munich, Germany.

*Corresponding author's email: Volker.Lohmann@med.uni-heidelberg.de

**Abstract**: RNA binding motif protein 39 (RBM39) is an RNA-binding protein involved in tumorigenesis, cell metabolism and development. Here, we performed a genome-wide CRISPR/Cas9 screen in two liver-derived cell lines and identified RBM39 as a regulator of cell intrinsic innate immune responses, affecting transcription and/or splicing of key pathway components, in particular interferon regulatory factor 3 (IRF3). Knockdown of *RBM39* or treatment with Indisulam, an aryl sulfonamide drug targeting RBM39 for proteasomal degradation, strongly reduced the induction of interferon-stimulated genes (ISGs) in response to double-stranded RNA (dsRNA), lipopolysaccharide (LPS) and viral infections mediated by IRF3. *RBM39* knockdown further restrained the type III interferon (IFN) pathway, by reducing

expression of the receptor subunit Interleukin 10 Receptor Subunit Beta (IL-10RB). RNAseq and mass spectrometry revealed altered expression of additional signaling factors, highlighting the importance of RBM39 in orchestrating innate immunity.

**One Sentence Summary:** RBM39 acts as a novel innate immune factor by regulating transcription and/or alternative splicing of IRF3 and several other key proteins involved in innate immune responses.

## INTRODUCTION

The cell intrinsic innate immune system belongs to the first line of host defense mechanisms protecting against invading pathogens. When infected, a limited number of host Pattern Recognition Receptors (PRRs) plays a vital role in recognizing several Pathogen-associated molecular patterns (PAMPs), which activate innate immune responses through complex signaling cascades to eliminate infections. Viral components, including viral DNA (*1, 2*), single-stranded RNA (ssRNA) (*3, 4*), double-stranded RNA (dsRNA) (*5, 6*) and virus-encoded proteins (*7*), are sensed by distinct PRRs. The recognition triggers the cell intrinsic innate immune response in infected cells. For instance, dsRNA, a replication intermediate of many RNA viruses, is sensed by cytosolic retinoic acid-inducible gene (RIG)-I-like receptors (RLRs, RIG-I and MDA5) (*5, 6, 8*) and endosomal Toll-like receptor 3 (TLR3) (*9*). These PRRs then recruit the adaptor proteins mitochondrial antiviral signaling protein (MAVS) and TIR domain containing adaptor molecule 1 (TRIF), respectively, activating a chain of kinases, E3 ubiquitin ligases and E2 ubiquitin-conjugating enzymes. This leads to nuclear factor kappa B subunit 1 (NF-κB) pathway activation and to production of pro-inflammatory cytokines or phosphorylating IRF3, leading to its dimerization and translocation from cytoplasm into nucleus. Subsequently, IRF3 binds to responsive promoters and induces transcription of type I/type III IFNs and interferon stimulated genes (ISGs). IFNs act in an auto- and paracrine manner, binding to their receptors, Interferon alpha and beta receptor (IFNAR) and Interferon Lambda Receptor (IFNLR), on the cell surface, respectively, but signaling via a common cascade upon phosphorylation of signal transducer and activator of transcription 1 and 2 (STAT1 and STAT2). Eventually, STATs form hetero- or homodimer and translocate into nucleus to accelerate ISG expression in infected and neighboring cells.

RNA binding-motif protein 39 (RBM39) (also known as HCC1.4 or CAPERα) was initially identified as an autoantigen in a hepatocellular carcinoma patient (*10*) and has been found to be upregulated in multiple cancer cells (*11-13*). It shares high similarity with the splicing factor U2AF 65 kDa subunit (U2AF65), and contains an N-terminal serine/arginine (SR)-rich domain followed by two RNA-recognition motifs (RRM) and a third C-terminal noncanonical RRM belonging to the U2AF homology motif (UHM) family which mediates the interaction with UHM-ligand motif (ULM) of U2AF65 (*14*). Previous studies have demonstrated that RBM39 functions as a coactivator of activating protein-1 (AP-1), Estrogen Receptor 1(ERα) and Estrogen Receptor 2 (ERβ) (*15-17*) and that it is involved in multiple biological processes, including cell cycle control (*18, 19*), cell metabolism (*19*) and tumorigenesis (*20, 21*), possibly through its splicing activity. In recent years, aryl sulfonamide drugs, such as Indisulam and E7820, were found to degrade RBM39 in a DDB1 and CUL4 associated factor 15 (DCAF15)-dependent manner and thus have been

widely investigated in anticancer research (*22-24*). While most studies on RBM39 so far focused on cancer cells, there is a limited knowledge of its function in immunity, with one *in vivo* study suggesting that Indisulam-mediated modulation of RBM39 enhances anti-tumor immunity (*25*).

In our study, RBM39 emerged as a prominent candidate through a CRISPR/Cas9-mediated screening in two liver-based cell lines aimed at identifying novel factors associated with the TLR3 response in hepatocytes. Our study reveals that RBM39 exerts a broader influence on innate immunity by modulating the transcription and splicing processes involved in the basal expression of IRF3 and other crucial factors in the interferon (IFN) signaling pathway. Based on the findings, it is plausible to consider that drugs targeting RBM39, such as Indisulam, may function as immunosuppressants in individuals undergoing treatment.

## RESULTS:

### A genome-wide CRISPR/Cas9 Screen identifies RBM39 as a novel factor contributing to TLR3 signaling.

The initial aim of this study was the identification of novel factors contributing to the regulation of cell intrinsic innate immune responses, in particular focusing on TLR3-mediated response in hepatocytes.

To establish a positive selection system, we developed a death reporter system expressing the suicide gene truncated BH3 Interacting Domain Death Agonist (tBID) under the transcriptional control of the interferon induced protein with tetratricopeptide repeats 1 (IFIT1) promoter (Fig. 1A). Upon activation of the TLR3 pathway, tBID expression is induced, resulting in apoptosis (*26*). For the screening we chose PH5CH (*27*), a non-neoplastic, immortalized hepatocyte cell line expressing all PRRs responsive to dsRNA, and Huh7-Lunet-TLR3 (*28*), a hepatocellular carcinoma (HCC)-derived cell line requiring ectopic expression of PRRs for efficient response to dsRNA. The tBID reporter was transduced into both cell lines for stable expression. To evaluate the approach, TLR3-specific stimulation was achieved by the addition of the synthetic dsRNA analog polyinosinic:polycytidylic acid (poly(I:C)) to the cell culture supernatant, leading to efficient tBID-associated, TLR3-dependent cell death only upon activation of the *IFIT1* promoter in both cell lines, in contrast to the empty vector (Fig. S1A). Subsequently, we transduced the IFIT1-tBID cell lines with lentiviral vectors encoding Cas9 along with the GeCKOv2.0 human genome-wide single guide RNA (sgRNA) library, that includes a total of 122,411 unique sgRNAs targeting 19,050 genes and 1,864 miRNAs (Fig. 1B). After selection, we added 50 µg/ml poly(I:C) to the medium to activate the TLR3 pathway, or PBS as a control. As a consequence, cells with an intact TLR3 pathway were killed due to the induction of tBID expression, whereas cells expressing guide RNAs targeting genes involved in TLR3 signaling survived, resulting in the enrichment of such sgRNAs. We then analyzed the sgRNA population of stimulated and non-stimulated cells at 72 hours post-stimulation by next-generation sequencing (NGS), to identify target genes interfering with the TLR3 pathway.

Candidate genes were determined by being enriched beyond a cell-line-specific threshold calibrated to yield about 2000 overrepresented sgRNAs for each cell line. Due to the expected

background of the screen, we needed to narrow down the enriched genes to obtain primary screen hits. We filtered primary candidate genes using a thresholding strategy that was calibrated to include three positive controls (TIR-domain-containing adapter-inducing interferon-β (TRIF), TLR3 and unc-93 homolog B1 (UNC93B1)) for each cell line (*29-31*). A gene was considered as a primary hit in case 5 out of 6 different sgRNAs found enriched in the poly(I:C) treated samples of at least one replicate and the presence of at least one sgRNA targeting a gene in 2 out of 3 replicates. After such filtering, 50 protein-coding genes were chosen for functional validation, except for 5 microRNAs which were excluded despite matching our criteria (Fig. S1B and Table S1). The protein-coding genes were validated by siRNA knockdown in Huh7-Lunet-TLR3 cells (Fig. 1C and D). However, knockdown of most candidates resulted in unimpaired or even upregulated TLR3 responses (Fig. 1C), likely due to a high background of surviving cells even in absence of sgRNAs (Fig. S1), resulting in non-specific enrichment. Only the knockdown of a few genes reduced the TLR3 response to levels comparable to the positive control (siUNC93B1). The four candidates with strongest phenotype, lysine demethylase 2A (KDM2A), protein tyrosine phosphatase receptor type T (PTPRT), cleavage and polyadenylation factor II subunit (PCF11) and RBM39 were chosen for further validation in PH5CH cells. Indeed, knockdown of these factors strongly attenuated innate immune responses (Fig. 1E). However, *PTPRT* mRNA turned out not to be detectable in Huh7 or PH5CH cells, arguing for off-target effects of the siRNA. PCF11 was not followed up due to its general role in termination of transcription (*32*). To exclude possible off-target effects for the remaining candidates, we designed siRNA-resistant mutants and expressed them in PH5CH cells via lentiviral transduction. The expression of KMD2A did not rescue TLR3 response (Fig. S1B). In contrast, the RBM39 siRNA-resistant mutant (RBM39.Esc) was able to rescue the phenotype of siRNA knockdown in PH5CH (Fig. 1F). In Huh7-Lunet-TLR3 cells, RBM39.Esc rescued the response slightly although not significantly (Fig. S2A).

Since PH5CH was considered the most authentic among the available hepatocyte models, due to its non-neoplastic nature, we decided to continue here with an in-depth analysis of the specific role of RBM39 in the TLR3 pathway.

**RBM39 is involved in multiple innate immune pathways and different cell lines**

To rule out that RBM39 might have an exclusive impact on IFIT1 expression, which so far served as the sole readout in our validation, we further analyzed modulation of other ISGs upon *RBM39* knockdown and TLR3 stimulation, including Interferon-Stimulated Protein, 15 KDa (ISG15), MX dynamin like GTPase 1 (MxA) and C-X-C motif chemokine ligand 10 (CXCL10) in PH5CH cells. All tested ISGs showed reduction in *RBM39*-silenced cells compared to the control, similar in magnitude to the one upon knockdown of *TRIF* (Fig. S2 B-D), suggesting that RBM39 has a broad impact on various ISGs. To confirm this on protein level, we additionally detected IFN-β expression via ELISA upon *RBM39* knockdown and observed a significant decline here as well (Fig. 2A). Given that Huh7.5 cells, a subclone of Huh7 (*33*), do not express functional PRRs, ectopic expression of retinoic acid inducible gene I (RIG-I) and Melanoma Differentiation-Associated Gene 5 (MDA5) allowed us to identify the function of RBM39 in other key innate immune pathways beyond TLR3 (*28*). Notably, silencing of *RBM39* decreased RIG-I and MDA5-mediated *IFIT1* mRNA expression upon transfection of poly(I:C) (Fig. 2B). To validate our finding in non-hepatic cell lines, we tested A549 cells, which are based on adenocarcinoma cells from human alveolar basal epithelium. These cells endogenously express RIG-I and MDA5, but not TLR3, and are regarded as innate immune-competent (*34*). Indeed, knockdown of *RBM39* in

A549 cells reduced *IFIT1* induction in response to poly(I:C) similarly as observed for PH5CH and Huh7 (Fig. 2C), demonstrating that RBM39's involvement in innate immunity is neither limited to hepatocytes, nor limited to TLR3 signaling alone. Since TLR3, RIG-I and MDA5 all recognize dsRNA, we wondered whether the function of RBM39 was only related to RNA recognition. Therefore, we stimulated PH5CH with lipopolysaccharide (LPS) to activate the TLR4 pathway, and again found a significant decline of *CXCL10* mRNA expression upon *RBM39* knockdown (Fig. 2D). Furthermore, considering that the activation of PRRs not only leads to production of various ISGs, but also triggers NF-κB signaling, resulting in the production of cytokines and chemokines, we investigated a potential involvement of RBM39 in the NF-κB pathway. However, the expression of two NF-κB-induced genes, TNF alpha induced protein 3 (TNFAIP3) and interleukin 6 (IL6) was not or only mildly affected in PH5CH cells upon poly(I:C) activation and *RBM39* knockdown (Fig. 2E), indicating a minor effect of RBM39 on the NF-κB pathway in these cells.

Our previous findings have confirmed that RBM39 affects the expression of IFNβ (Fig. 2A), suggesting its involvement in the induction of IFN expression upstream of the Janus kinase (JAK)-STAT pathway. However, stimulation of PH5CH with IFN2α was not affected by RMB39 knockdown (Fig. 2F), whereas the response to IFNλ1 was drastically impaired (Fig. 2G), suggesting that RBM39 might additionally target the type III IFN pathway. Given that type I and type III IFNs share the same JAK-STAT signaling cascade, but diverge in their interaction with the receptors interferon alpha and beta receptor (IFNAR) and interferon lambda receptor (IFNLR), respectively, we measured the mRNA expression of the two IFNLR subunits, namely interferon lambda receptor 1 (*IFNLR1*) and interleukin 10 receptor subunit beta (*IL10RB*). Interestingly, *IFNLR1* mRNA expression was increased upon RBM39 knockdown, while *IL10RB* expression was significantly diminished (Fig. 2H), suggesting that RBM39 specifically affects type III IFNs activation by modulating the transcription of *IL10RB*.

Considering RBM39's role in both upstream (Fig. 2A) and downstream (Fig. 2G) signaling of the type III IFN pathway, we investigated whether the IFNλ receptor was the main contributor to the suppression of innate immune pathways mediated by *RBM39* knockdown. However, knockdown of *RBM39* in A549 IFNAR/IFNLR receptor knockout cells had a similar impact on *IFIT1* (Fig. 2I, left) and *IFNβ* mRNA induction (Fig. 2I, right) as observed in wild-type A549 cells (Fig. 2C). These findings suggest that the reduced expression of the IFNλ receptor may not play a dominant role in RBM39-mediated regulation of innate immune responses, at least not under the experimental conditions of our study, measuring ISG induction at 6 h after stimulation, thereby mainly focusing on the primary induction of ISGs.

Overall, our results suggest that RBM39 is involved in the direct induction of IFNβ and ISGs upon stimulation with dsRNA and LPS, but has a minor influence on NF-κB signaling. We also showed that RBM39 regulates the type III IFN pathway, by governing expression of the *IL10Rβ* receptor chain.

**RBM39 regulates IRF3 expression to modulate innate immune responses**

In order to elucidate the mechanism involved in RBM39-mediated regulation of IFN and ISG induction, we firstly examined the phosphorylation of IRF3, a key event mediating IFN and ISGs production upon PRR activation by dsRNA. As expected, phosphorylated-IRF3 (p-IRF3) levels

were low in non-stimulated cells and significantly enhanced upon poly(I:C) stimulation (Fig. 3A, left). Intriguingly, *RBM39* knockdown not only resulted in a remarkable decrease in p-IRF3, but also in significant reduction of total IRF3 protein levels, suggesting a regulation of the constitutive expression of IRF3 (Fig. 3A).

Indisulam is a sulfonamide drug mediating the interaction between the E3 ligase DCAF15 and RBM39, leading to the ubiquitination and proteasomal degradation of RBM39 (*22, 35, 36*). To further validate the impact of RBM39 on IRF3 expression, we treated PH5CH cells with Indisulam. Indeed, RBM39 protein levels were reduced in Indisulam-treated cells in a dose-dependent manner, concomitant with lower IRF3 abundance and some cytopathic effect at higher concentrations (Fig. 3B). In order to verify whether IRF3 depletion upon Indisulam treatment was mediated by RBM39, we made use of an RBM39 mutant (G268V) reported to confer partial resistance to Indisulam (*22*). Overexpression of RBM39 G268V partially rescued RBM39 Indisulam-mediated degradation and thus restored IRF3 expression compared to cells expressing wild-type RBM39 (Fig. S3A). These results confirmed that Indisulam affected IRF3 expression by targeting RBM39.

Similar results were obtained in A549 cells (Fig. S3B) and in primary human hepatocytes (PHH) (Fig. 3C), with the latter indicating that the RBM39-mediated IRF3 depletion also appeared in primary cells, albeit associated with substantial cytotoxicity at higher concentrations (Fig. 3C). In contrast, RBM39 was refractory to Indisulam treatment in primary mouse hepatocytes (PMH) (Fig. S3C), probably due to the lack of expression of murine DCAF15 or resistance to Indisulam (*37*), in line with the lack of cytotoxicity (Fig. S3C, right).

Altogether, our results demonstrated that RBM39 governs basal expression of IRF3, thereby exerting a crucial role in the activation of innate immune responses.

## The innate immune function of RBM39 during virus infection

So far, our study mainly relied on stimulation of cell intrinsic innate immune responses using the synthetic dsRNA analog poly(I:C). To investigate the function of RBM39 in innate immunity in more physiological settings, we performed virus infection experiments with four viruses known to induce strong innate immune responses mediated by IRF3.

Sendai Virus (SeV) is a model virus sensed by RIG-I (*38*). Knockdown of *RBM39* in A549 cells indeed resulted in a strong reduction of *IFIT1* mRNA expression, comparable to the one upon *MAVS* knockdown (Fig. 4A, left). In turn, virus replication was significantly enhanced by both conditions (Fig. 4A, right). Similar results were obtained for infection of A549 cells with Rift Valley Fever Virus (RVFV) upon Indisulam treatment, resulting in reduced *IFIT1* mRNA induction (Fig. 4B, left), whereas viral RNA replication was not significantly increased (Fig. 4B, right). We further analyzed two hepatotropic viruses with a more restricted tropism, using derivatives of HepG2 cells known to give rise to robust innate immune responses (*8, 28*). We again used Indisulam treatment to modulate RBM39/IRF3 expression. As expected, hepatitis E virus (HEV) infection of HepG2/C3A strongly increased *IFIT1* mRNA levels, which was significantly reduced by Indisulam (Fig. 4C, left). Here, virus replication was only mildly impacted by the reduced innate immune response, probably due to the relative resistance of HEV replication to IFN (*39, 40*) (Fig. 4C, right). Similarly, *IFIT1* mRNA induction upon hepatitis D

virus (HDV) infection in HepG2 cells reconstituted with the essential HDV entry receptor NTCP was significantly downregulated by Indisulam treatment (Fig. 4D, left), here resulting in a slight but significant increase in viral replication (Fig. 4D, right).

Overall, our data demonstrate that RBM39 substantially contributes to the cell intrinsic innate immune response to viral infections.

## RBM39 governs the transcription and splicing of IRF3 mRNA

To understand how RBM39 affects IRF3 expression, we firstly investigated a potential direct impact on protein stability. We overexpressed ectopically the coding sequence (CDS) of IRF3 in PH5CH IRF3 KO cells (PH5CH-eIRF3), which allowed us to investigate a possible impact of RBM39 on translation or protein stability. Indeed, knockdown of *RBM39* had no effect on IRF3 abundance upon IRF3 ectopic expression in PH5CH-eIRF3 cells (Fig. 5A), whereas, as expected, IRF3 protein level was reduced in PH5CH naïve cells upon the same treatment. Importantly, ectopic expression of IRF3 restored the *IFIT1* mRNA induction upon *RBM39* knockdown (Fig. 5B), supporting our conclusion that IRF3 was the key factor contributing to the suppression of innate immune responses caused by *RBM39* knockdown, at least upon TLR3 stimulation.

Next, we investigated whether RBM39 was involved in splicing or transcriptional regulation of *IRF3* mRNA. Silencing of RBM39 (Fig. 5C, right) significantly decreased *IRF3* mRNA expression (Fig. 5C, left), suggesting a role in transcriptional regulation. We therefore analyzed the impact of RMB39 on the activity of the *IRF3* promoter (*41*) using a luciferase reporter plasmid (Fig. 5D), revealing a slight but significant reduction in relative luciferase activity expressed from the full-length and the core *IRF3* promoter (Fig. 5E). This result supported the contribution of RBM39 to transcription of *IRF3* mRNA, albeit the magnitude of the effect did not match with the reduction on IRF3 protein amounts (Fig.3A). Therefore, we assessed the potential impact of RBM39 on splicing of *IRF3* mRNA, since several alternatively spliced isoforms of *IRF3* mRNA had been reported (*42, 43*). To this end, we modulated RBM39 abundance by knockdown or Indisulam treatment in PH5CH cells, and subjected the total RNA to RNA sequencing (RNAseq) analysis. While *GAPDH* total mRNA levels were not affected by any of the conditions, as expected (Fig, 6A), *RBM39* RNA abundance was significantly reduced upon the knockdown, but, surprisingly, strikingly increased upon Indisulam treatment (Fig. 6B), hinting at a possible self-regulation of *RBM39* mRNA levels by protein abundance. Consistent with RT-qPCR results, RNA-seq showed around 20% reduction in *IRF3* mRNA read counts in both conditions (Fig. 6C), albeit lacking statistical significance. Remarkably, we observed substantial, consistent changes in splicing of *IRF3* mRNA when RBM39 was suppressed either by siRNA or by Indisulam treatment (Fig. 6D). Among the *IRF3* isoforms, *IRF3-203* is known to play a functional role in innate immunity, while other isoforms either encode different amino acid sequences or were degraded by nonsense-mediated decay (NMD) due to exon skipping or intron retention. Particularly, *IRF3-228* has been reported to have an inhibitory effect on innate immune activation (*43*). Our results showed a significant decrease of the functional *IRF3-203* isoform and increased relative (Fig. 6D) and absolute (Fig. S4A) abundance of other isoforms, such as *IRF3-228*, *IRF3-202* and *IRF3-219*, in siRBM39- or Indisulam-treated PH5CH cells. In addition, we conducted RT-qPCR using primers specifically targeting each of the *IRF3* isoforms that are detected in RNAseq (Fig. 6E) and obtained very similar results upon *RBM39* knockdown (Fig. 6F).

In summary, we showed that the combined effect of RBM39 on transcription and splicing of *IRF3* mRNA resulted in the reduction of basal IRF3 protein expression.

## Global transcriptome, splicing and proteome analysis highlights the role of RBM39 in innate immunity

We next aimed for a comprehensive proteomic and transcriptomic analysis, to identify other components of innate immunity affected by RBM39, comparing the impact of siRNA mediated *RBM39* knockdown and of Indisulam treatment.

For the proteomic analysis we found 135 proteins in *RBM39* knockdown samples and 225 proteins in Indisulam-treated samples with significant changes (fold change < 0.5 or > 2, p-value <0.05) (Fig. 7A and Table S2). RBM39 was among the most significantly changed proteins, as expected (Fig. 7A and S5A). In contrast, changes in IRF3 levels were not significant (Fig. S5B), despite the profound differences we saw in western blot, pointing at the limited sensitivity of the analysis. An additional caveat was the inability to differentiate peptides derived from functional or non-functional proteins synthesized by alternatively spliced RNAs. Also, the low number of overlapping hits upon the knockdown and Indisulam treatment (Fig. 7A, Table S2), with many additional factors barely reaching significance, argued for the moderate coverage of the data, precluding a more extensive bioinformatic analysis. Notably, we still identified 3 additional factors contributing to the cell intrinsic innate immune response, with STAT1 and STAT2 significantly depleted in both conditions (Fig. 7A, Fig. S5C, D, Table S2), and RIG-I levels strongly reduced upon Indisulam treatment (Fig. 7A, Fig. S5E, Table S2).

Due to the complex, multifactorial mode of action of RBM39 in transcription and splicing, we analyzed the RNAseq dataset in the context of differentially expressed genes (DEG) and differential transcript usages (DTUs), indicative for changes in splicing, comparing knockdown of *RBM39* and Indisulam treatment. Our analysis identified 4007 DEGs (fold change < 0.5 or > 2, p-value <0.05) and 4053 DTUs (p-value >0.05) in *RBM39* knockdown and Indisulam-treated samples. 1570 DEGs and 1977 DTUs overlapped in both conditions (39% and 49% of total events, respectively) (Fig. 7B, Table S3 and Table S4), arguing for the reliability of the analysis. For DEGs, 585 genes were upregulated and 978 genes were downregulated in both conditions (Fig. 7C), overall revealing similar numbers as previous transcriptomic studies (*21, 23, 44, 45*). Still, not all candidate genes significantly modulated by knockdown of RBM39 / Indisulam treatment are necessarily direct targets of RBM39. For example, growth arrest and DNA-damage-inducible 34 (GADD34) and activating transcription factor 3 (ATF3), regulators of the integrated cellular stress response, were among the most significantly upregulated genes in both conditions (Fig. S6A and B), indicating that lack of RBM39 induces cellular stress, likely contributing to collateral changes in the transcriptional program.

In line with literature, Gene Ontology (GO)-analysis conveyed that many metabolic pathways were most significantly affected by modulation of RBM39 abundance (Fig. 7D), while innate immunity was not (Fig. S6C), explaining why previous studies might have missed this aspect so far. Importantly and in agreement with the proteomic data, we found additional factors involved in the cell intrinsic innate immune response (Fig. 7E, Table S5). Regarding the IRF3-induced pathway (Fig. S6D), the cytosolic dsRNA sensors *RIG-I* and *MDA5* were significantly downregulated, with *RIG-I* showing changes in both transcriptional and splicing regulation (Fig.

8A, Fig. 7E), whereas *MDA5* expression was mainly decreased at transcriptional level, with one minor splice variant vanishing in addition (Fig. 8B). The TLR3 adaptor *TRIF* was downregulated as well, but to a lower degree, reaching significance only upon Indisulam treatment (Fig. 8C). At this point, we aimed to address the relevance of other factors regulated by RBM39 beyond IRF3 in the induction of the IFN pathway. While the impact of *TRIF* modulation to the TLR3 pathway was unlikely, due to the rescue of TLR3 response by ectopic IRF3 expression (Fig. 5B), additional contributions of *RIG-I* and *MDA5* appeared possible. We therefore bypassed the regulation of IRF3 by overexpressing it in PH5CH cells (PH5CH-eIRF3), and used BafilomycinA (BafA), an inhibitor of endosomal acidification, to prevent TLR3 activation. Indeed, IRF3 expression did not suffice to restore *IFIT1* mRNA induction upon RBM39 knockdown and poly(I:C) transfection (Fig. 8D), suggesting that regulation of *RIG-I* and *MDA5* expression further contributes to the impact of RBM39 on innate immune responses.

For the interferon response pathway (Fig. S6D), the DEG analysis was consistent with our previous RT-qPCR data for the IFNλ receptor (Fig. 2H) and showed the same reduction for *IL10RB* and induction for *IFNLR1* in both conditions (Fig. 8E and F, left), in absence of differential splicing (Fig. 8E and F, right). Surprisingly, we found a similar pattern for the regulation of the type I IFN receptor with *IFNAR1* expression upregulated and *IFNAR2* significantly downregulated, the latter with additional changes in the splicing pattern (Fig. 8G and H), although we previously found no phenotypic impact of *RBM39* knockdown of IFN2α treatment (Fig. 2F). In line with the proteomic data, also *STAT1* and *STAT2* expression was strongly reduced upon RBM39 depletion, in both cases associating with changes in differential splicing (Fig. 8I and J).

All in all, our RNA-seq and proteome analysis identified several additional key factors of the IFN response beyond IRF3 and IL10RB affected by RBM39, further supporting the crucial role of RBM39 in regulation of innate immunity.

## DISCUSSION

Genome-wide CRISPR/Cas9 screens present a powerful tool to study host factors of innate immunity mostly in immune cells, such as macrophages (*46*), dendritic cells (*47*), or in the more commonly used Hela cells (*48*) and HEK 293T cells (*49*). In our study, we applied this approach in two liver cell lines, Huh7 and PH5CH, and specifically targeted the TLR3 pathway by poly(I:C) supernatant feeding. Eventually, we identified RBM39 as a novel factor not only affecting TLR3 signaling, but having a broad impact on the cell intrinsic innate immune response by regulating the basal expression of IRF3 and other important pathway components.

RBM39 is a factor involved in splicing and transcriptional regulation of many genes, particularly contributing to tumorigenesis (*20, 21, 50*), cell cycle control (*12, 19*) and metabolism (*19*), but so far its role in innate immunity has not been shown. Paradoxically, a previous study indicated that porcine reproductive and respiratory syndrome virus (PRRSV) infection upregulated porcine RBM39 expression, resulting in dephosphorylation of c-Jun, downregulating AP-1 signaling (*51*). Additionally, studies have reported that some viruses regulate splicing factors like RBM10 and U5 spliceosomal RNA (snRNA) as an evasion strategy (*52, 53*). While RBM39 has previously been shown to interact with the viral NF-κB homolog v-Rel, inhibiting its activation,

the interplay between RBM39 and other human host NF-κB members like p50 and p105 has not been explored. Indeed, in our study, RBM39 had no impact on the NF-κB-induced gene induction, but only on genes regulated by IRF3. Here, we identified basal expression of *IRF3* as a key factor of cell intrinsic innate immune responses being modulated by knockdown of *RBM39* and Indisulam-mediated RBM39 degradation. This resulted in significantly impaired activation upon both dsRNA administration and virus infection. IRF3 regulation, on both transcriptional level and on splicing level, resulted in a switch from functional to non-functional isoforms. In addition, we identified additional pathway components being modulated by RBM39, including the PRRs RIG-I and MDA5, IL-10RB, IFNAR2, STAT1 and STAT2, all contributing to the reduced activation of cell intrinsic innate immune response regulated via IRF3.

The complexity of regulatory functions mediated by RBM39 might explain why other transcriptomic and proteomic analyses missed its role in innate immunity so far (*22, 23, 44, 54-57*). Knockdown of *RBM39* by siRNA and Indisulam treatment showed a wide degree of overlap in the transcriptomic and proteomic hits, respectively, arguing for the specificity of Indisulam towards RBM39 in the liver-derived cell lines used in our study and in agreement with previous studies (*55, 58*). However, we found little overlap between transcriptomic and proteomic analysis, probably due to the fact that the proteomics did not allow a distinction between different isoforms of each protein generated by alterative splicing (*59*). Overall, the transcriptomic analysis was in our hands more prone to identify innate immune response factors regulated by RBM39. While we could demonstrate that changes in IRF3, as well as RIG-I/MDA5 expression contributed to the induction of cell intrinsic innate immune response, the data were more complex in the case of IFN treatment. Type I and type III IFNs bind to different receptors, but engage identical signaling pathways (*60*). We observed reduced expression of *IL10RB*, *IFNAR2*, *STAT1* and *STAT2*, all essential for signal transduction, with STAT1 and STAT2 being involved in the response pathway to type I and type III IFNs (*60*). However, we found that only the type III response was functionally impaired by *RBM39* knockdown. It has been shown that IFN-β can form a high-affinity complex with IFNAR1, contributing to its potency and allowing for IFNAR2-independent signaling (*61, 62*). This might also be true, to some extent, for IFN-α. Thereby, the upregulation of *IFNAR1* expression upon *RBM39* knockdown/Indisulam treatment might compensate for the effect of the decreased STAT1/STAT2 and IFNAR2 expression. Still, the impact of RBM39 depletion on type I/III IFN responses might differ in various cell culture models and organs, depending on the expression levels of affected components of the pathway. In addition, further systemic effects of RBM39 ablation on innate immune responses are possible due to the complex involvement of IL-10RB in several cytokine receptor complexes, responding not only to IFNλ, but also to pro- and anti-inflammatory cytokines including IL-10, IL-22 and IL-28/29 (*63, 64*).

RBM39 depletion was shown to have a strong anti-proliferative impact, which might explain our failure to obtain RBM39 knockout clones in PH5CH cells (not shown). This growth inhibitory effect has put forward RBM39 as a promising target for cancer therapy and contributed to numerous clinical trials implementing aryl sulfonamides like Indisulam, albeit yet with limited success, likely due to the lack of predictive markers (*65*). In contrast, Indisulam showed high activity in preclinical models like mice engrafted with human tumors (*66*) and, more recently, in neuroblastoma models (*23, 66*), associated with limited toxicity. Indisulam treatment of all human hepatic cells tested in our study, including two cancer cell lines (HepG2 and Huh7), one

non-neoplastic cell line (PH5CH), and PHH, resulted in a significant degradation of RBM39, albeit at varying doses. Although *RBM39* protein expression was similar in all these cell lines, PHH could be less sensitive to Indisulam due to lower *DCAF15* expression levels, critical for its mode of action. Importantly, RBM39 degradation was associated with a certain degree of cytotoxicity in all of our cell culture models. In contrast, Indisulam treatment of PMH had no impact on RBM39 and IRF3 expression and lacked obvious cytotoxicity. The different Indisulam sensitivity of PHH and PMH therefore imposes particular caution in interpreting toxicity data obtained in animal models. This is consistent with data showing only a minor effect of Indisulam treatment on RBM39 expression in different organs of mice, including the liver, with significant changes only in murine kidney and the engrafted human tumors (*22*, *45*, *66*).

The lack of Indisulam activity in PMH further precluded *in vivo* testing regarding immunosuppressive activities *in vivo*. Currently available aryl sulphonamides might generally not be suitable for clinical use as immunosuppressors, due to their focus on anti-cancer activity. However, substances targeting RBM39 to proteasomal degradation based on alternative E3 ligases beyond DCAF15 might be envisaged, as well as alternative tailored depletion strategies like molecular glues and proteolysis targeting chimeras (PROTACs) (*67*). In light of our data defining RBM39 as a regulator of key components of cell intrinsic innate immunity, it could be regarded as a candidate target to mitigate excessive innate immune responses contributing to viral pathogenesis (*68*) or autoimmune diseases (*69*).

## MATERIALS AND METHODS

### Study design

The aim of this study was to identify novel factors that are involved in intrinsic innate immune response in hepatocytes. Genome-wide CRISPR/Cas9 screen was performed in two hepatic cell lines (PH5CH cells with endogenous TLR3 expression and Huh-Lunet cells ectopically expressing TLR3) and identified RBM39 as a novel innate immune factor. To understand the role of RBM39 in innate immune signaling, the down-regulation of RBM39 was achieved by siRNA silencing and Indisulam-mediated degradation. Poy(I:C), LPS, IFNs stimulation and virus infection were used to stimulate cells and ISGs were analyzed by RT-qPCR, ELISA and western blot. Luciferase assay, RNA-seq and mass spectrometry were performed, intensive bioinformatic analysis was followed to further elucidate the mechanism underlying the regulatory function of RBM39 on cell intrinsic innate immunity.

### Cell culture:

PH5CH cells were a generous gift from K. Shimotohno. Huh 7.5 cells were a kind gift from Charles Rice. A549 cell were obtained from ATCC, A549 IFNAR/LR KO cells (*70*), Huh7-Lunet cells (*71*), Huh7.5-RIG-I and Huh7.5-MDA5 (*28*), HepG2-NTCP (*72*) have been described before. HepG2/C3A were obtained from ATCC. Primary human hepatocytes (PHH) were purchased from BioIVT and cultured in William E media containing 1% (v/v) Glutamax, 1% (v/v) Non-Essential Amino Acids, 1% (v/v) penicillin/streptomycin (all from Gibco, Germany), 0.2% (v/v) normocin (Invivogen, USA), 2% (v/v) B27 (Gibco, Germany), 1% (v/v) N2 supplement (Gibco, Germany), 100 mM nicotinamide (Sigma-Aldrich, USA), 1.25 mM N-

acetylcysteine (Sigma-Aldrich, USA), 10 µM Y27632 (Peprotech, USA), 1 µM A83-01 (Tocris, UK).

Cells, unless specifically mentioned, were cultured in Dulbecco's Modified Eagle Medium (Life Technologies, Darmstadt, Germany) supplemented with 10% fetal bovine serum, nonessential amino acids (Life Technologies), 100 U/mL penicillin, and 100 ng/mL streptomycin (Life Technologies) and cultivated at 37°C and 5% CO2. PH5CH-KDM2A, PH5CH-RBM39.Esc, PH5CH-RBM39 G268V, PH5CH-eIRF3 cells were kept under selection pressure of 1 mg/mL G418 (Geneticin) (Life Technologies, USA), Huh7-Lunet-TLR3, Huh7.5-RIG-I, HepG2-NTCP cells were maintained under selective pressure of 1 µg/mL puromycin (Sigma-Aldrich, Germany), Huh7.5-MDA5 cells were kept under the antibiotic pressure of 5 µg/mL blasticidin (Sigma-Aldrich, Germany).

**CRISPR/Cas9 knockout screening:**

For genome-wide CRISPR/Cas9 screen, PH5CH and Huh7-Lunet-TLR3 cells were transduced with lentiviral vectors containing the tBID death reporter and Cas9 (lentiCRISPRv2). Neomycin and puromycin were added for selection. After that, PH5CH and Huh7-Lunet-TLR3 cells stably expressing the tBID death reporter and Cas9 were transduced with lentiviral vectors containing the GeCKOv2.0 human genome-wide sgRNA library (Addgene, USA) at MOI=0.3. The GeCKOv2.0 human genome-wide sgRNA library includes a total of 122,411 unique sgRNAs targeting 19,050 genes (with 6 sgRNAs per gene) and 1,864 miRNAs (with 4 sgRNAs per miRNA) and a total number of 1,000 different non-targeting sgRNAs as controls.

After 24 hours, puromycin was added for selection. On day 7 post-transduction, 50ug/ml poly (I:C) or PBS as control were added to the medium to exclusively activate the TLR3 pathway. The experiments were performed in 2 independent biological replicates with 2 technical replicates each. Surviving cells were collected at 72 h post-stimulation, genomic DNA was extracted using NucleoSpin Blood L kit (Macherey-Nagel, Germany) according to manufacturer´s instructions. Amplicons were amplified and barcoded by PCR, purified again via agarose gel separation and using NucleoSpin Gel and PCR Clean-up kit (Macherey-Nagel, Germany), before being pooled and submitted to GATC Biotech (Germany), for Illumina NGS (Illumina HiSeq, 50 bp single reads, 240 million reads total, 20% PhiX DNA).

NGS data first was de-multiplexed to allocate the respective reads in the pooled population to each sample. Reads were counted for each gRNA in every sample, and then normalized to the total number of reads in this sample as well as the complexity sample taken one day after transduction of the lentiviral library, yielding normalized read counts.

Mean values of normalized read counts of the 4 technical replicates were generated for each of the 4 conditions. Based on mean values, fold changes were calculated between poly(I:C)- and PBS-treated samples. gRNAs with a higher fold change than a threshold were considered as primary hits. The threshold was adjusted for each cell line to yield the about 2000 top-ranked gRNAs for each experiment. Thresholds were 2.5x change in Huh-7-Lunet-TLR3 cells and 7x in tPH5CH cells. Preliminary hits were furthermore filtered for occurrences of at least 5

upregulated gRNAs per gene in all datasets combined, and the occurrence of at least one gRNA per gene in at least 3 independent datasets.

**Drug treatments:**

Poly(I:C) stimulation: Poly (I:C) (HMW) was used (Invivogen, USA) following the manufacturer's instructions. To specifically trigger TLR3, 50 µg/ml poly (I:C) were added directly into the medium. For TLR3, RIG-I and MDA5 stimulation, transfection was performed with 0.5 µg/ml poly (I:C) mixed with Lipofectamine2000 (Thermo Fisher Scientific, USA) in OptiMEM (Gibco, USA) according to the manufacturer's instructions. After 20min incubation at room temperature (RT), the mixture was added into the medium. Cells were stimulated for 6 h or 8 h, then harvested for RNA or protein extraction.

LPS stimulation: 1 µg/ml of LPS (Invivogen, Germany) was added into the medium. Cells were stimulated for 24 h and collected for RNA extraction.

Indisulam treatment: Indisulam was utilized (Sigma Aldrich, Germany) solved in DMSO at a final stock concentration of 10 mM. Indisulam, or same amount of DMSO as control, were added to the cell medium at the indicated concentrations; cells were incubated for the indicated time and treated further with either poly (I:C) or virus infection. At the indicated time points, cells were harvested for RNA extraction or protein analysis.

IFNs stimulation: IFN2α and IFNλ1 were purchased from PBL, USA and Peprotech, USA, respectively. 200 IU/ml IFN2α and 10ng/ml IFNλ1 were added to the medium. Cells were stimulated for 24 h and collected for RNA extraction.

Bafilomycin A1 treatment: Cells were treated with 10nM Bafilomycin A1 (BafA), purchased from Sigma Aldrich and solved according to the manufacturer's instructions. BafA was added to the cell medium 45 minutes before poly (I:C) stimulation at a concentration of 10nM.

**Real time quantitative PCR:**

Total RNA was isolated from cultured cells using the NucleoSpin RNA Plus kit (Macherey-Nagel, Germany). RT-qPCR was performed as described before (*28*). For gene expression analysis, cDNA as generated from RNA samples using High-Capacity cDNA Reverse Transcription Kit (Thermo Fisher Scientific, USA), and was used for qPCR analysis with the 2x iTaq Universal SYBR Green Supermix (Bio-Rad, Germany). Reactions were performed on a CFX96 Touch Real-Time PCR Detection System (Bio-Rad, Germany) as follows: 95°C for 3 minutes, 95°C for 10 and 60°C for 30 seconds. mRNA fold change was calculated normalizing on Glyceraldehyde-3-phosphate dehydrogenase (GAPDH) mRNA expression relative to untreated / uninfected / mock transfected cells. For IRF3 isoforms mRNA measurement, cDNA was prepared by reverse transcription kit (Thermo Fisher Scientific, USA) using oligo(dT)18 primers (Thermo Scientific, Germany). mRNA expression fold change was normalized on GAPDH and Hydroxymethylbilane synthase (HMBS) expression levels relative to siNT-transfected cells. Primers IRF3-228+203 were designed to target both IRF3-228 and IRF3-203

stretches, other IRF3 primers were designed to target specific exons or introns of individual isoforms. IRF3-203 mRNA expression was calculated by subtracting the expression of IRF3-228 from that of IRF3-228 + IRF3-203. All qPCR primers are listed in Table S6.

**Western blot:**

Cells were lysed in protein lysis buffer (50mM TRIS HCl pH7.4, 150mM NaCl, 1% Triton-X 100, protease inhibitor) on ice for 45min. Cell lysates were then centrifuged at 14,000 g for 15 minutes at 4 °C to exclude cell debris. Supernatants were collected and mixed with 6x Lämmli buffer (0.375M Tris-HCl, 9% SDS, 50% Glycerol, 0.03% Bromophenol Blue, 9% β-mercaptoethanol), boiled at 95°C for 5 minutes and cooled down on ice for 2 minutes. Samples were separated by 10% SDS-PAGE and then blotted onto polyvinylidene difluoride (PVDF) membranes (Merk Millipore, Germany). Membranes were then blocked with 5% milk in PBST (0.05% Tween) or 5% BSA in TBST (0.01% Tween) and incubated with the indicated antibodies. Membranes were imaged via the ECL Plus Western Blotting Detection System (Pierce, GE Healthcare, Little Chalfont, UK) according to the instructions of the manufacturer. Signal was recorded using the Advance ECL Chemocam Imager (Intas Science Imaging, Germany). Quantification of western blot was performed by Fiji.

**Lentivirus preparation and transduction:**

5 x $10^6$ HEK293T cells were seeded in 10 cm dishes 16 hours before transfection. The next day, the target plasmid (5.14 µg) together with pCMV-Gag-Pol (5.14 µg) and pMD2-VSVG (1.71 µg) were mixed in 400µl OptiMEM (Gibco, USA). 364 µl of OptiMEM were separately mixed with 36µl polyethylenimine (PEI). The two mixtures were merged and incubated for 20 min at RT, and then added to the cells as previously described (*73*). After 2 days, lentivirus was collected and filtered at 0.45 nm filter (Sigma Aldrich, Germany) to exclude cell debris, and store at -80 °C or used for transduction. PH5CH-eIRF3 stable cells were produced by transduction of lentiviral particles encoding for IRF3 under control of the Rosa26 promoter (IRF3 sgRNA resistant mutant) as previously described (*28*) in the abovementioned PH5CH IRF3 KO cells. PH5CH-KDM2A, PH5CH-RBM39.Esc, PH5CH-RBM39 G268V were generated by lentiviral transduction of particles containing corresponding plasmids.

**Cell Viability Assay:**

Cell viability upon transduction of tBID death reporter was assessed in 96-well plates through WST-1 assay (Roche, Switzerland) according to the manufacturers' instructions. Cell viability of Indisulam-treated cells was accessed by CellTiter-Glo® 2.0 Assay (Promega, Germany) according to the manufacturer's instructions.

**ELISA:**

Supernatants were collected from stimulated cells, IFNβ protein levels were measured by LumiKineTMXpress hIFN-β 2.0 (InvivoGen, Germany) according to the manufacturer's instructions.

**Luciferase reporter assay:**

pGL3-982 or pGL3-149 Firefly reporter, together with pRL-CMV Gaussia (Promega, USA) reporter as reference were transfected into PH5CH RBM39 knockdown cells using Lipofectamine2000 (Thermo Fisher Scientific, USA) according to the manufacturer's instructions. After 24 h, cells were lysed by addition of Luciferase lysis buffer (1% Triton X-100, 25mM Glycyl Glycin, 15mM MgSO4, 4mM EGTA, 10% Glycerol, pH7.8, 10mM DTT) and luciferase activity (Relative Ligh Units, RLU) was measured by a Mitras LB940 luminometer (Berthold Technologies, Germany). RVFV-RLuc assay was performed as described before (doi.org/10.3390/cells10102600). At 24 hours after infection, infected cells were washed once with PBS and immediately lysed with luciferase lysis buffer. Cell lysates were stored frozen at -80°C to ensure proper lysis and the Renilla luciferase signal was measured by injecting 300 µl of luciferase assay buffer (15 mM $K_3PO_4$ [pH7.8], 25 mM Glycyl-Glycin [pH 7.8], 15 mM $MgSO_4$, 4 mM EGTA) supplemented with 1.43 coelenterazine (102173, PJK, Germany) followed by read-out of the signal with a 480 nm high-sense filter (480m20BREThs, Berthold) using the Mitras2 multimode plate reader (LB942, Berthold).

**RNA sequencing (RNA seq)**

RNA-Sequencing and RNA quality control was performed by the Genomics and Proteomics Core facility of the German cancer research centre using the Illumina Hiseq NovaSeq 6000 with RNA seq reads in 2 x 100 bp format. For sample preparation, 1.5 x $10^5$ cells were seeded in a 6-well plate. Cells were either transfected with siRBM39 or siNT as control, or treated with 1mM Indisulam or the same amount of DMSO as control. 48 hours after transfection, cells were lysed and total RNA was extracted via NucleoSpin RNA Plus kit (Macherey-Nagel, Germany) following the manufacturer's instructions. RNA was quantified using OD measurement at 260 nm.

Human reference transcriptome (Human Gencode v40) mapping and quantification of the transcripts were performed using the salmon package with GC bias correction (*74*). Differential expression analysis was performed using DESeq2 (*75*), and DTU analysis was performed with DRIMseq (*76*). Analysis of the TLR3, RIG-I and MDA5 pathway was based on the KEGG annotation and performed using GAGE (*77*). GO analysis was performed using the GOstats package (*78*).

**Virus infection:**

For Sendai virus (SeV) infection upon RBM39 knockdown, 6 x $10^4$ A549 cells were transfected with siRNA RBM39. After 48 h, the cells were infected with SeV (MOI=1) in PBS with 0.3% BSA at room temperature (RT). One hour after infection, cells were washed with phosphate-buffered saline (PBS) and complete medium was added. Cells were collected after 24 h for further analysis.

For Rift Valley Fever Virus (RVFV) infection, 2 x $10^4$ A549 cells were seeded into 24-well plates. The following day, cells were treated with 0.1M Indisulam or DMSO for 48 hours, and then inoculated with RVFV-RLuc at a MOI of 0.01 in DMEM with 2% FCS. After 24 hours of infection, cells washed once with PBS, lysed in 100 µl of luciferase lysis buffer, and frozen at -80 °C for further analysis.

For hepatitis E virus (HEV) (Genotype 3 Kernow C1 P6 accession number: JQ679013, a kind gift from Suzanne Emerson, NIH) (*79*) and hepatitis D virus (HDV) infection, 2.5 x $10^4$ HepG2/C3A cells and HepG2-NTCP cells, respectively, were seeded in collagen (Corning, USA)-coated plates and treated with 0.1 µM Indisulam or same amount of DMSO for 48h. Subsequently, cells were infected with HEV (MOI=4) in MEM with 10% FBS or HDV (MOI=4) in DMEM with 1.5% DMSO, 4% PEG. 24 hours after infection, cells were washed with PBS. Cells were incubated for 5 days and collected for further analysis.

**Statistical analysis:**

Independent biological replicates are denoted with n-numbers. To test for significance, two-tailed unpaired Welch's test, were performed using GraphPad Prism 8 software (GraphPad Software, La Jolla, CA, USA). *p <0.05; **p <0.01; ***p <0.001; ****p <0.0001.

**Supplementary Materials**

Fig. S1 tBID death reporter, NGS data processing and rescue of KDM2A

Fig. S2 RBM39 plays function in other cell line and for other ISGs

Fig. S3 Indisulam treatment in PH5CH-RBM39 G268V, A549 cells and PMH

Fig. S4 Absolute RNA counts of siRBM39 or Indisulam-treated PH5CH cells

Fig. S5 Protein expression of some innate immune factors in proteomic analysis

Fig. S6 mRNA expression of some innate immune factors in transcriptomic analysis and GO, KEGG analysis

Table S1 Candidate list in CRISPR/Cas9 screen

Table S2 Proteomic analysis of mass spectrometry

Table S3 DEG analysis of RNA seq

Table S4 DTU analysis of RNA seq

Table S5 DEG and DTU analysis for innate immune factors in RNA seq

Table S6 Primers and antibodies

**References and Notes**

1. N. C. Di Paolo *et al.*, Virus binding to a plasma membrane receptor triggers interleukin-1 alpha-mediated proinflammatory macrophage response in vivo. *Immunity* **31**, 110-121 (2009).

2. A. Krug *et al.*, TLR9-dependent recognition of MCMV by IPC and DC generates coordinated cytokine responses that activate antiviral NK cell function. *Immunity* **21**, 107-119 (2004).
3. F. Heil *et al.*, Species-specific recognition of single-stranded RNA via toll-like receptor 7 and 8. *Science* **303**, 1526-1529 (2004).
4. S. A. Nicholas, V. V. Sumbayev, The involvement of hypoxia-inducible factor 1 alpha in Toll-like receptor 7/8-mediated inflammatory response. *Cell Res* **19**, 973-983 (2009).
5. D. Goubau *et al.*, Antiviral immunity via RIG-I-mediated recognition of RNA bearing 5 '-diphosphates. *Nature* **514**, 372-+ (2014).
6. L. Gitlin *et al.*, Essential role of mda-5 in type I IFN responses to polyriboinosinic:polyribocytidylic acid and encephalomyocarditis picornavirus. *Proc Natl Acad Sci U S A* **103**, 8459-8464 (2006).
7. E. A. Kurt-Jones *et al.*, Herpes simplex virus 1 interaction with Toll-like receptor 2 contributes to lethal encephalitis. *Proc Natl Acad Sci U S A* **101**, 1315-1320 (2004).
8. N. Gillich, Z. Zhang, M. Binder, S. Urban, R. Bartenschlager, Effect of variants in LGP2 on MDA5-mediated activation of interferon response and suppression of hepatitis D virus replication. *J Hepatol* **78**, 78-89 (2023).
9. M. Yamamoto *et al.*, Role of adaptor TRIF in the MyD88-independent toll-like receptor signaling pathway. *Science* **301**, 640-643 (2003).
10. H. Imai, E. K. Chan, K. Kiyosawa, X. D. Fu, E. M. Tan, Novel nuclear autoantigen with splicing factor motifs identified with antibody from hepatocellular carcinoma. *J Clin Invest* **92**, 2419-2426 (1993).
11. A. H. Sillars-Hardebol *et al.*, CSE1L, DIDO1 and RBM39 in colorectal adenoma to carcinoma progression. *Cell Oncol (Dordr)* **35**, 293-300 (2012).
12. I. Mercier *et al.*, CAPER, a novel regulator of human breast cancer progression. *Cell Cycle* **13**, 1256-1264 (2014).
13. Y. Chai *et al.*, Overexpression of HCC1/CAPERalpha may play a role in lung cancer carcinogenesis. *Tumour Biol* **35**, 6311-6317 (2014).
14. G. A. Stepanyuk *et al.*, UHM-ULM interactions in the RBM39-U2AF65 splicing-factor complex. *Acta Crystallogr D Struct Biol* **72**, 497-511 (2016).
15. D. J. Jung, S. Y. Na, D. S. Na, J. W. Lee, Molecular cloning and characterization of CAPER, a novel coactivator of activating protein-1 and estrogen receptors. *J Biol Chem* **277**, 1229-1234 (2002).
16. D. H. Dowhan *et al.*, Steroid hormone receptor coactivation and alternative RNA splicing by U2AF65-related proteins CAPERalpha and CAPERbeta. *Mol Cell* **17**, 429-439 (2005).
17. S. Mai *et al.*, Functional interaction between nonreceptor tyrosine kinase c-Abl and SR-Rich protein RBM39. *Biochem Biophys Res Commun* **473**, 355-360 (2016).
18. N. Faherty *et al.*, Negative autoregulation of BMP dependent transcription by SIN3B splicing reveals a role for RBM39. *Sci Rep* **6**, 28210 (2016).
19. Y. K. Kang *et al.*, CAPER is vital for energy and redox homeostasis by integrating glucose-induced mitochondrial functions via ERR-alpha-Gabpa and stress-induced adaptive responses via NF-kappaB-cMYC. *PLoS Genet* **11**, e1005116 (2015).
20. G. Huang, Z. Zhou, H. Wang, E. S. Kleinerman, CAPER-alpha alternative splicing regulates the expression of vascular endothelial growth factor(1)(6)(5) in Ewing sarcoma cells. *Cancer* **118**, 2106-2116 (2012).
21. E. Wang *et al.*, Targeting an RNA-Binding Protein Network in Acute Myeloid Leukemia. *Cancer Cell* **35**, 369-384 e367 (2019).
22. T. Han *et al.*, Anticancer sulfonamides target splicing by inducing RBM39 degradation via recruitment to DCAF15. *Science* **356**, (2017).
23. A. Nijhuis *et al.*, Indisulam targets RNA splicing and metabolism to serve as a therapeutic strategy for high-risk neuroblastoma. *Nat Commun* **13**, 1380 (2022).
24. T. Uehara *et al.*, Selective degradation of splicing factor CAPERalpha by anticancer sulfonamides. *Nat Chem Biol* **13**, 675-680 (2017).
25. S. X. Lu *et al.*, Pharmacologic modulation of RNA splicing enhances anti-tumor immunity. *Cell* **184**, 4032-4047 e4031 (2021).
26. K. Huang *et al.*, Cleavage by Caspase 8 and Mitochondrial Membrane Association Activate the BH3-only Protein Bid during TRAIL-induced Apoptosis. *J Biol Chem* **291**, 11843-11851 (2016).
27. M. Ikeda *et al.*, Human hepatocyte clonal cell lines that support persistent replication of hepatitis C virus. *Virus Res* **56**, 157-167 (1998).
28. O. Colasanti *et al.*, Comparison of HAV and HCV infections in vivo and in vitro reveals distinct patterns of innate immune evasion and activation. *J Hepatol*, (2023).

29. E. Meylan *et al.*, Cardif is an adaptor protein in the RIG-I antiviral pathway and is targeted by hepatitis C virus. *Nature* **437**, 1167-1172 (2005).
30. L. Alexopoulou, A. C. Holt, R. Medzhitov, R. A. Flavell, Recognition of double-stranded RNA and activation of NF-kappaB by Toll-like receptor 3. *Nature* **413**, 732-738 (2001).
31. K. Pelka *et al.*, The Chaperone UNC93B1 Regulates Toll-like Receptor Stability Independently of Endosomal TLR Transport. *Immunity* **48**, 911-922.e917 (2018).
32. K. Kamieniarz-Gdula *et al.*, Selective Roles of Vertebrate PCF11 in Premature and Full-Length Transcript Termination. *Mol Cell* **74**, 158-172.e159 (2019).
33. K. J. Blight, J. A. McKeating, C. M. Rice, Highly permissive cell lines for subgenomic and genomic hepatitis C virus RNA replication. *J Virol* **76**, 13001-13014 (2002).
34. Y. Li *et al.*, SARS-CoV-2 induces double-stranded RNA-mediated innate immune responses in respiratory epithelial-derived cells and cardiomyocytes. *Proc Natl Acad Sci U S A* **118**, (2021).
35. D. E. Bussiere *et al.*, Structural basis of indisulam-mediated RBM39 recruitment to DCAF15 E3 ligase complex. *Nat Chem Biol* **16**, 15-23 (2020).
36. T. C. Ting *et al.*, Aryl Sulfonamides Degrade RBM39 and RBM23 by Recruitment to CRL4-DCAF15. *Cell Rep* **29**, 1499-1510 e1496 (2019).
37. B. V. Mistry *et al.*, Expression profiling of WD40 family genes including DDB1- and CUL4- associated factor (DCAF) genes in mice and human suggests important regulatory roles in testicular development and spermatogenesis. *BMC Genomics* **21**, 602 (2020).
38. L. Martínez-Gil *et al.*, A Sendai virus-derived RNA agonist of RIG-I as a virus vaccine adjuvant. *J Virol* **87**, 1290-1300 (2013).
39. D. Todt *et al.*, Antiviral Activities of Different Interferon Types and Subtypes against Hepatitis E Virus Replication. *Antimicrob Agents Chemother* **60**, 2132-2139 (2016).
40. X. Wu *et al.*, Pan-Genotype Hepatitis E Virus Replication in Stem Cell-Derived Hepatocellular Systems. *Gastroenterology* **154**, 663-674.e667 (2018).
41. H. G. Xu, W. Ren, C. Lu, G. P. Zhou, Characterization of the human IRF-3 promoter and its regulation by the transcription factor E2F1. *Mol Biol Rep* **37**, 3073-3080 (2010).
42. C. Li, L. Ma, X. Chen, Interferon regulatory factor 3-CL, an isoform of IRF3, antagonizes activity of IRF3. *Cell Mol Immunol* **8**, 67-74 (2011).
43. A. Y. Karpova, L. V. Ronco, P. M. Howley, Functional characterization of interferon regulatory factor 3a (IRF-3a), an alternative splice isoform of IRF-3. *Mol Cell Biol* **21**, 4169-4176 (2001).
44. S. Mai *et al.*, Global regulation of alternative RNA splicing by the SR-rich protein RBM39. *Biochim Biophys Acta* **1859**, 1014-1024 (2016).
45. P. K. Puvvula *et al.*, Inhibiting an RBM39/MLL1 epigenomic regulatory complex with dominant-negative peptides disrupts cancer cell transcription and proliferation. *Cell Rep* **35**, 109156 (2021).
46. A. J. Chui *et al.*, N-terminal degradation activates the NLRP1B inflammasome. *Science* **364**, 82-85 (2019).
47. O. Parnas *et al.*, A Genome-wide CRISPR Screen in Primary Immune Cells to Dissect Regulatory Networks. *Cell* **162**, 675-686 (2015).
48. R. Fang, Q. Jiang, X. Jia, Z. Jiang, ARMH3-mediated recruitment of PI4KB directs Golgi-to-endosome trafficking and activation of the antiviral effector STING. *Immunity* **56**, 500-515.e506 (2023).
49. R. Fang *et al.*, Golgi apparatus-synthesized sulfated glycosaminoglycans mediate polymerization and activation of the cGAMP sensor STING. *Immunity* **54**, 962-975.e968 (2021).
50. J. Dutta, G. Fan, C. Gelinas, CAPERalpha is a novel Rel-TAD-interacting factor that inhibits lymphocyte transformation by the potent Rel/NF-kappaB oncoprotein v-Rel. *J Virol* **82**, 10792-10802 (2008).
51. Y. Song *et al.*, RBM39 Alters Phosphorylation of c-Jun and Binds to Viral RNA to Promote PRRSV Proliferation. *Front Immunol* **12**, 664417 (2021).
52. B. Pozzi *et al.*, Dengue virus targets RBM10 deregulating host cell splicing and innate immune response. *Nucleic Acids Res* **48**, 6824-6838 (2020).
53. S. Boudreault *et al.*, Reovirus mu2 protein modulates host cell alternative splicing by reducing protein levels of U5 snRNP core components. *Nucleic Acids Res* **50**, 5263-5281 (2022).
54. E. Wang *et al.*, Targeting an RNA-Binding Protein Network in Acute Myeloid Leukemia. *Cancer Cell* **35**, 369-384.e367 (2019).
55. T. C. Ting *et al.*, Aryl Sulfonamides Degrade RBM39 and RBM23 by Recruitment to CRL4-DCAF15. *Cell Rep* **29**, 1499-1510.e1496 (2019).
56. Z. Dou *et al.*, Indisulam exerts anticancer effects via modulation of transcription, translation and alternative splicing on human cervical cancer cells. *Am J Cancer Res* **13**, 2922-2937 (2023).

57. S. Coomar *et al.*, Overlaid Transcriptional and Proteome Analyses Identify Mitotic Kinesins as Important Targets of Arylsulfonamide-Mediated RBM39 Degradation. *Mol Cancer Res*, Of1-of11 (2023).
58. T. Uehara *et al.*, Selective degradation of splicing factor CAPERα by anticancer sulfonamides. *Nat Chem Biol* **13**, 675-680 (2017).
59. B. C. Carlyle *et al.*, Isoform-Level Interpretation of High-Throughput Proteomics Data Enabled by Deep Integration with RNA-seq. *J Proteome Res* **17**, 3431-3444 (2018).
60. H. M. Lazear, J. W. Schoggins, M. S. Diamond, Shared and Distinct Functions of Type I and Type III Interferons. *Immunity* **50**, 907-923 (2019).
61. N. A. de Weerd *et al.*, Structural basis of a unique interferon-β signaling axis mediated via the receptor IFNAR1. *Nat Immunol* **14**, 901-907 (2013).
62. N. A. de Weerd *et al.*, A hot spot on interferon α/β receptor subunit 1 (IFNAR1) underpins its interaction with interferon-β and dictates signaling. *J Biol Chem* **292**, 7554-7565 (2017).
63. S. Mukhopadhyay *et al.*, Loss of IL-10 signaling in macrophages limits bacterial killing driven by prostaglandin E2. *J Exp Med* **217**, (2020).
64. S. Mossner *et al.*, Synthetic interleukin 22 (IL-22) signaling reveals biological activity of homodimeric IL-10 receptor 2 and functional cross-talk with the IL-6 receptor gp130. *J Biol Chem* **295**, 12378-12397 (2020).
65. Y. Xu, A. Nijhuis, H. C. Keun, RNA-binding motif protein 39 (RBM39): An emerging cancer target. *Br J Pharmacol* **179**, 2795-2812 (2022).
66. S. Singh *et al.*, Targeting the spliceosome through RBM39 degradation results in exceptional responses in high-risk neuroblastoma models. *Sci Adv* **7**, eabj5405 (2021).
67. L. M. Luh *et al.*, Prey for the Proteasome: Targeted Protein Degradation-A Medicinal Chemist's Perspective. *Angew Chem Int Ed Engl* **59**, 15448-15466 (2020).
68. M. M. Aboudounya, R. J. Heads, COVID-19 and Toll-Like Receptor 4 (TLR4): SARS-CoV-2 May Bind and Activate TLR4 to Increase ACE2 Expression, Facilitating Entry and Causing Hyperinflammation. *Mediators Inflamm* **2021**, 8874339 (2021).
69. H. Kato, T. Fujita, RIG-I-like receptors and autoimmune diseases. *Curr Opin Immunol* **37**, 40-45 (2015).
70. S. S. Burkart *et al.*, High-resolution kinetic characterization of the RIG-I-signaling pathway and the antiviral response. *Life Sci Alliance* **6**, (2023).
71. P. Backes *et al.*, Role of annexin A2 in the production of infectious hepatitis C virus particles. *J Virol* **84**, 5775-5789 (2010).
72. K. Giersch *et al.*, Hepatitis delta virus persists during liver regeneration and is amplified through cell division both in vitro and in vivo. *Gut* **68**, 150-157 (2019).
73. O. Grünvogel *et al.*, DDX60L Is an Interferon-Stimulated Gene Product Restricting Hepatitis C Virus Replication in Cell Culture. *J Virol* **89**, 10548-10568 (2015).
74. R. Patro, G. Duggal, M. I. Love, R. A. Irizarry, C. Kingsford, Salmon provides fast and bias-aware quantification of transcript expression. *Nat Methods* **14**, 417-419 (2017).
75. M. I. Love, W. Huber, S. Anders, Moderated estimation of fold change and dispersion for RNA-seq data with DESeq2. *Genome Biol* **15**, 550 (2014).
76. M. Nowicka, M. D. Robinson, DRIMSeq: a Dirichlet-multinomial framework for multivariate count outcomes in genomics. *F1000Res* **5**, 1356 (2016).
77. W. Luo, M. S. Friedman, K. Shedden, K. D. Hankenson, P. J. Woolf, GAGE: generally applicable gene set enrichment for pathway analysis. *BMC Bioinformatics* **10**, 161 (2009).
78. S. Falcon, R. Gentleman, Using GOstats to test gene lists for GO term association. *Bioinformatics* **23**, 257-258 (2007).
79. P. Shukla *et al.*, Cross-species infections of cultured cells by hepatitis E virus and discovery of an infectious virus-host recombinant. *Proc Natl Acad Sci U S A* **108**, 2438-2443 (2011).

**Acknowledgments:** The authors thank Rahel Klein, Ulrike Herian for excellent technical assistance. We thank Charles M. Rice for Huh7.5 cells and Kunitada Shimotohno for PH5CH cells. We also need to thank the Genomics and Proteomics Core facility of the German Cancer Research Centre for the RNA-seq sample measurement. Additionally, we thank Zhenfeng Zhang, Julia Welsch, Jun-gen Hu, Zhaozhi Sun for providing reagents, and Cong Si Tran and Minh-Thu Pham for helpful discussions.

**Funding:** This work was supported by the Deutsche Forschungsgemeinschaft (DFG, German Research Foundation) – project number 272983813 – TRR 179, to VL, MB, AP, DW, RB, MS, SU and VLDT. VL received additional DFG funding, project number 519777725. TL was supported by the China Scholarship Council. VLDT was supported by DZIF-TTU Hepatitis Projects 05.823, MB and VGM were supported by DFG BI1693/1-2. NAR is a holder of a Georg Forster Research Fellowship for Experienced Researchers from the Alexander von Humboldt Foundation.

**Author contributions:**

Conceptualization: VL, TL, OG, JT

Methodology: VL, OG, OC, NAR, GEG, AKM

Investigation: TL, AL, JT, SMOU, PR, VGM, APir, ES, RQ, AB, HEH, JP,

Visualization: TL, PR, OG, JT,

Funding acquisition: VL

Project administration: VL

Supervision: VL, AP, RB, MB, DW, MS, MM, SU, VLDT

Writing – original draft: TL, OC, VL

Writing – review & editing: all authors

**Competing interests:** Authors declare that they have no competing interests.

**Data and materials availability:** Details related to materials and methods are provided in the Supplementary material. Further data supporting the findings of this study is available upon request. Please contact the corresponding author.

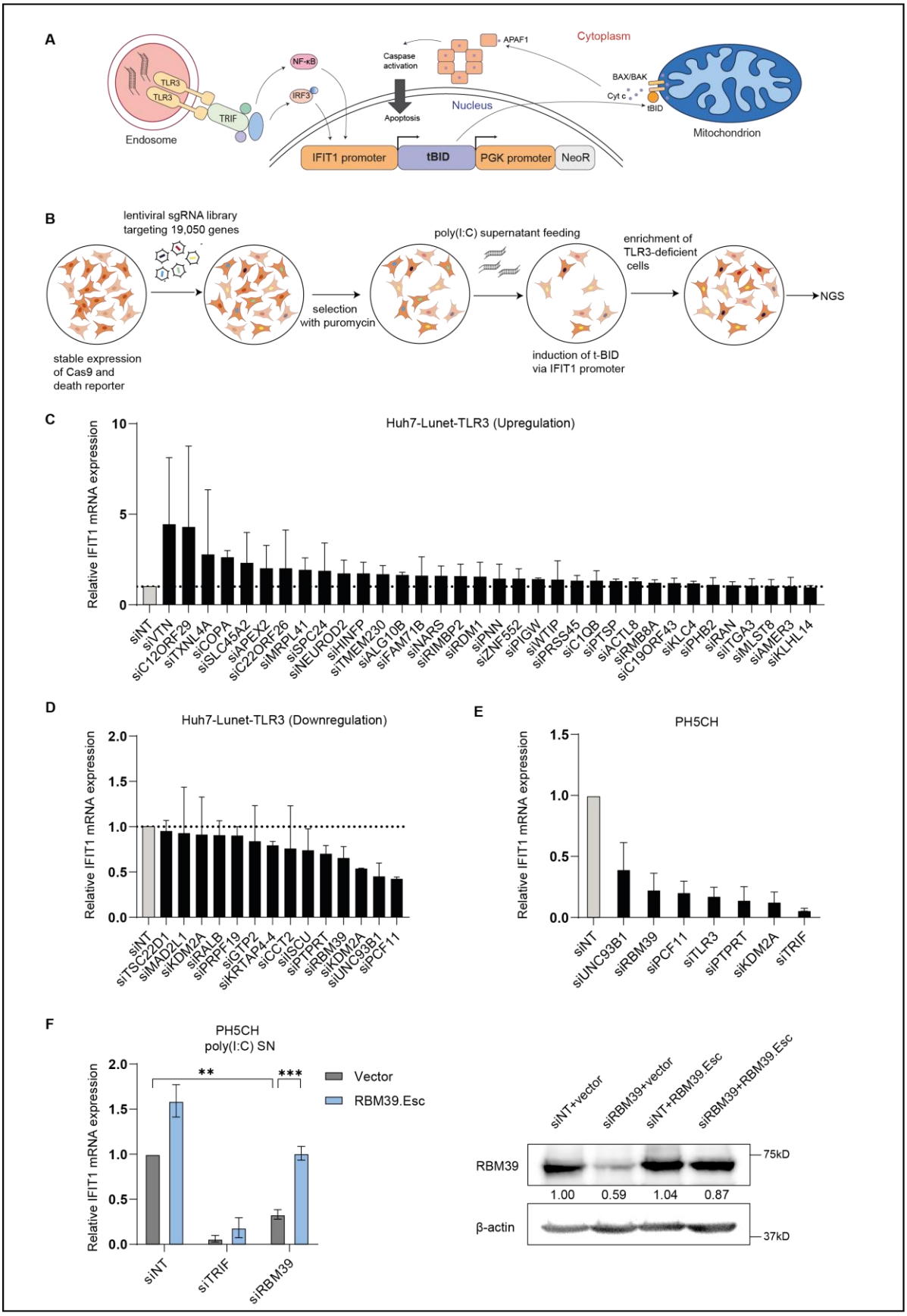
A
Endosome
TLR3
TLR3
TRIF
NF-κB
IRF3
Caspase activation
APAF1
Cytoplasm
BAX/BAK
Cyt c
tBID
Mitochondrion
Apoptosis
Nucleus
IFIT1 promoter
tBID
PGK promoter
NeoR
B
lentiviral sgRNA library targeting 19,050 genes
stable expression of Cas9 and death reporter
selection with puromycin
poly(I:C) supernatant feeding
induction of t-BID via IFIT1 promoter
enrichment of TLR3-deficient cells
NGS
C
Huh7-Lunet-TLR3 (Upregulation)
Relative IFIT1 mRNA expression
siNT
siVTN
siC12ORF29
siTXNL4A
siCOPA
siSLC45A2
siAPEX2
siC22ORF26
siMRPL41
siSPC24
siNEUROD2
siHINFP
siTMEM230
siALG10B
siFAM71B
siNARS
siRIMBP2
siRDM1
siPNN
siZNF552
siPIGW
siWTIP
siPRSS45
siC1QB
siPTSP
siACTL8
siRMB8A
siC19ORF43
siKLC4
siPHB2
siRAN
siITGA3
siMLST8
siAMER3
siKLHL14
D
Huh7-Lunet-TLR3 (Downregulation)
Relative IFIT1 mRNA expression
siNT
siTSC22D1
siMAD2L1
siKDM2A
siRALB
siPRPF19
siGTP2
siKRTAP4-4
siCCT2
siSCU
siPTPRT
siRBM39
siKDM2A
siUNC93B1
siPCF11
E
PH5CH
Relative IFIT1 mRNA expression
siNT
siUNC93B1
siRBM39
siPCF11
siTLR3
siPTPRT
siKDM2A
siTRIF
F
PH5CH
poly(I:C) SN
Relative IFIT1 mRNA expression
**
***
Vector
RBM39.Esc
siNT
siTRIF
siRBM39
siNT+vector
siRBM39+vector
siNT+RBM39.Esc
siRBM39+RBM39.Esc
RBM39
75kD
1.00
0.59
1.04
0.87
β-actin
37kD

**Fig. 1. Genome-wide CRISPR/Cas9 screen identifies potential TLR3 related factors.**

(**A**) Schematic of the lentiviral truncated BID (tBID) death reporter system. The tBID expression is driven by the IFIT1 promoter, while the expression of the neomycin selection marker (NeoR) is under the control of the constitutive PGK promoter. Working principle: (1) dsRNA is taken up via endocytosis and transported to the endosome. (2) The endosomal TLR3 recognizes dsRNA and triggers signaling via TRIF, resulting in activation of the transcription factors IRF3 and NF-κB. (3) Activated transcription factors induce expression of tBID by binding the IFIT1 promoter. (4) tBID associates with Bcl-2 proteins BAX and BAK to form a complex that permeabilizes the outer mitochondrial membrane and mediates release of Cytochrome c (Cyt c) into the cytoplasm. (5) Cyt c binds APAF1, triggering its oligomerization and binding to Pro-Caspase-9. Activated Caspase-9 in turn activates Caspases-3 and -7, inducing apoptosis. (**B**) Workflow of the CRISPR/Cas9 screen. PH5CH and Huh7 Lunet-TLR3 stably expressing the death reporter and Cas9 were transduced with the genome-wide lentiviral CRISPR sgRNA library and selected with puromycin for stable expression. TLR3 stimulation with poly(I:C) induced expression of tBID and thus apoptosis in case of intact TLR3 signaling. Then, surviving TLR3-deficient cells were enriched and collected for Next Generation Sequencing (NGS). (**C** to **E**) 50 candidate genes were selected and subjected to siRNA validation. The individual candidate genes were silenced through siRNA for 48 h, and then the cells were stimulated by 50 µg/ml poly (I:C) supernatant feeding for 8 h. IFIT1 mRNA was measured by qPCR. Knockdown of the candidates up-regulated (**C**) or down-regulated (**D**) *IFIT1* mRNA expression in Huh7 Lunet-TLR3 cells. Knockdown of *RBM39, PCF11, PTPRT* and *KDM2A* in PH5CH cells reduced *IFIT1* mRNA expression in PH5CH cells (**E**). siUNC93B1, siTLR3 and siTRIF were used as positive controls. Data are from two biological replicates (n = 2). (**F**) RBM39 rescue experiment. PH5CH cells expressing RBM39.Esc or empty vector were transfected with siRBM39 or siNT/siTRIF as controls for 48 h, and then fed with 50 µg/ml poly (I:C) in the supernatant for 6 h. IFIT1 mRNA was measured by qPCR (left), RBM39 expression was measured by western blot (right). Relative expression to siNT-treated samples was normalized on GAPDH. Data are from three biological replicates (n = 3), error bars indicate standard deviation (SD). Statistical significance was assessed through Welsch's unpaired *t*-test.

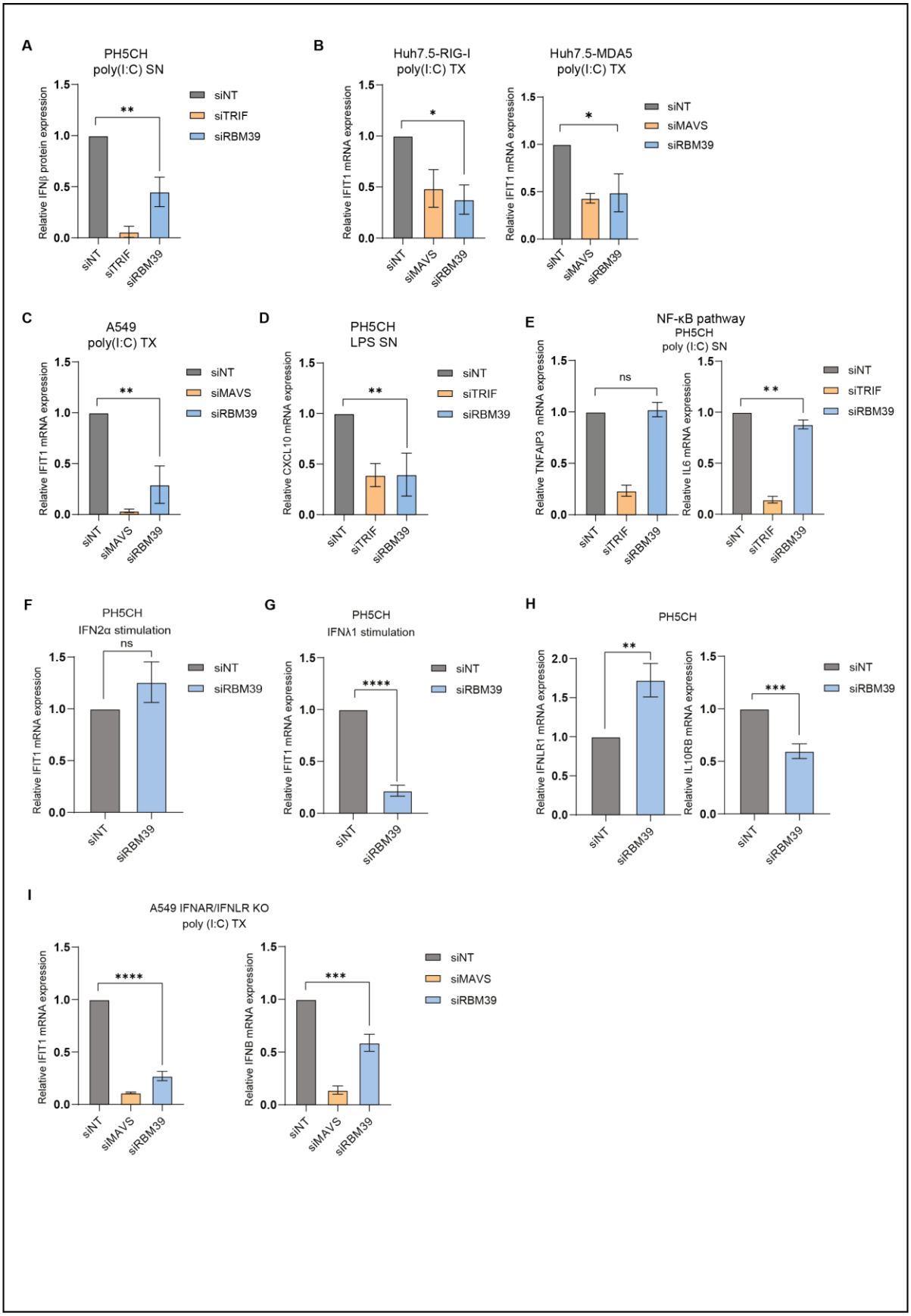
A
PH5CH
poly(I:C) SN
Relative IFNβ protein expression
siNT
siTRIF
siRBM39
B
Huh7.5-RIG-I
poly(I:C) TX
Huh7.5-MDA5
poly(I:C) TX
Relative IFIT1 mRNA expression
siNT
siMAVS
siRBM39
C
A549
poly(I:C) TX
D
PH5CH
LPS SN
Relative CXCL10 mRNA expression
E
NF-κB pathway
PH5CH
poly (I:C) SN
Relative TNFAIP3 mRNA expression
Relative IL6 mRNA expression
ns
F
PH5CH
IFN2α stimulation
G
PH5CH
IFNλ1 stimulation
H
PH5CH
Relative IFNLR1 mRNA expression
Relative IL10RB mRNA expression
I
A549 IFNAR/IFNLR KO
poly (I:C) TX
Relative IFNB mRNA expression

**Fig. 2. RBM39 participates in multiple pathways and functions in various cell lines.**

(**A**) PH5CH cells were transfected with siRNA for 48h and then fed with 50 μg/ml poly(I:C) in the supernatant for 6 h. IFNβ protein secreted in the medium was measured by ELISA. (**B** and **C**) Huh7.5 cells with ectopic RIG-I (left) or MDA5 (right) expression, and A549 cells (**C**) were transfected with siRBM39 or siNT/siMAVS as control for 48 h and then transfected with 0.5 μg/ml poly (I:C) for 6 h. *IFIT1* mRNA was measured by qPCR. (**D**) PH5CH cells were transfected with siRBM39 or siNT/siTRIF as control for 48 h and then stimulated with 100 ng/ml LPS for 24 h. *CXCL10* mRNA was measured by qPCR. (**E**) PH5CH cells were transfected with siRBM39 or siNT/siTRIF as controls for 48 h and then fed with 50 μg/ml poly (I:C) for 6 h. TNFAIP3 (left) and IL6 (right) mRNA were measured by qPCR. (**F** and **G**) PH5CH cells were transfected with siRBM39 or siNT as control for 48 h and then stimulated with IFN2α (**F**) or IFNλ1 (**G**) for 24 h. *IFIT1* mRNA was measured by qPCR. (**H**) PH5CH cells were transfected with siRBM39 or siNT as control for 48 h. *IFNLR1* (left) and *IL10RB* (right) mRNA were measured by qPCR. (**I**) A549 IFNAR/IFNLR knockout cells were transfected with siRBM39 or siNT/siMAVS as controls for 48 h and then transfected with 0.5 μg/ml poly (I:C) for 6 h. *IFIT1* (left) and *IFNB1* (right) mRNA expression levels were measured by qPCR. Relative expression to siNT control was shown, mRNA fold change was normalized on *GAPDH*. Data are obtained from three biological replicates (n = 3), error bars refer to SD. Statistical significance was assessed through Welsch's unpaired *t*-test.

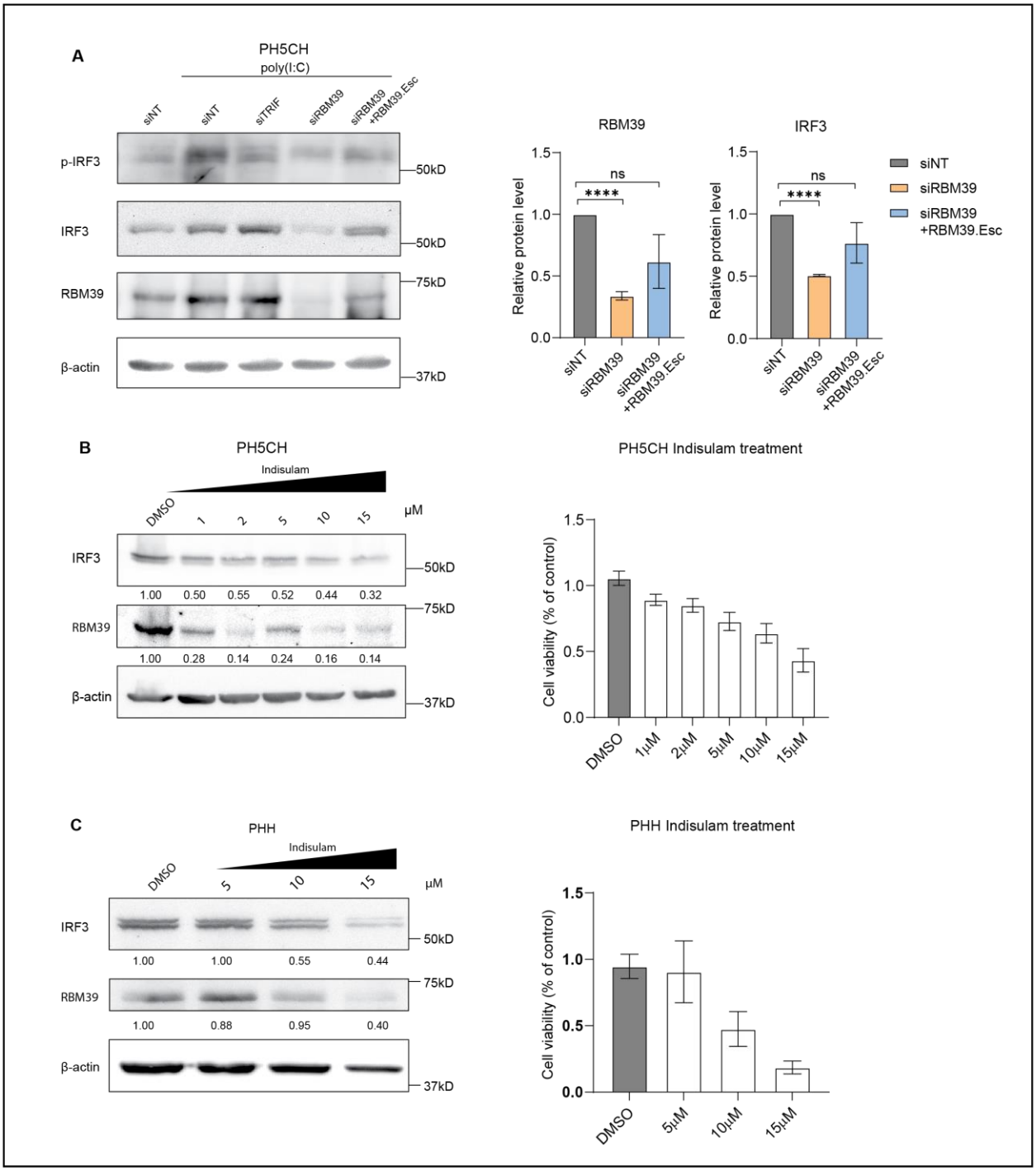


**Fig. 3. RBM39 controls the basal level of IRF3.**

(**A**) PH5CH cells or PH5CH RBM39.Esc cells were transfected with siRBM39 or siNT/siTRIF as controls for 48 h and then fed with 50 μg/ml poly (I:C) for 6 h. Phosphorylated IRF3 (p-IRF3), IRF3, RBM39 and β-actin protein expression levels were assessed by western blot (left). Quantification of three biological replicates was shown (right). (**B**) PH5CH cells and (**C**) PHH were treated with increasing concentrations of Indisulam as indicated. IRF3, RBM39 and β-actin protein expression levels were detected through immunoblotting (left). Cell viability was

measured via CellTiter-Glo®luminescent cell viability assay (right). Quantification of three independent experiments was expressed as average and is shown under each band. Protein expression was normalized on β-actin, relative protein levels to siNT or DMSO control were shown. Data shown are from three biological replicates (n = 3), error bars indicate SD. Statistical significance was assessed through Welsch's unpaired *t*-test.

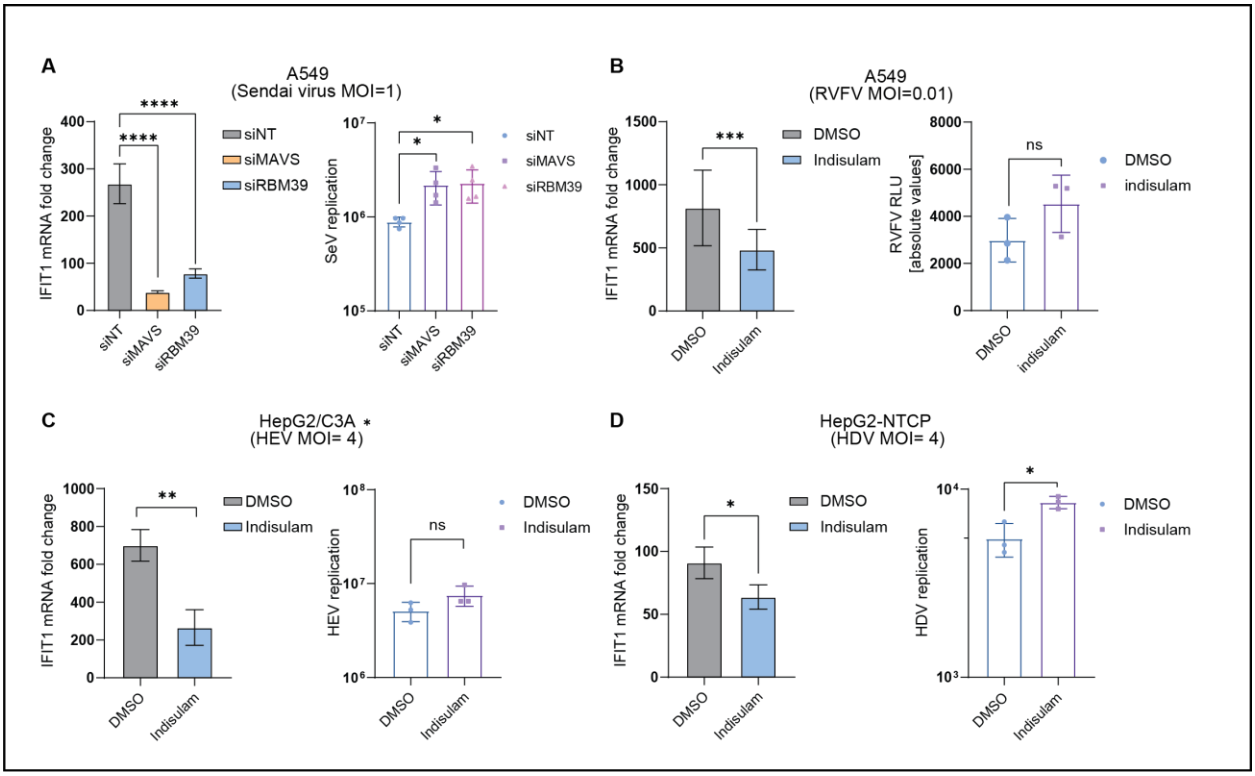


**Fig. 4. The innate immune regulation of RBM39 in virus infection models.**

(**A**) A549 cells were transfected with siRBM39 or siNT/siMAVS as control. 48 hours after transfection, cells were infected with Sendai virus (MOI= 1) for 24 h. *IFIT1* mRNA (left) and Sendai virus P protein mRNA (right) were measured through qPCR. (**B** to **D**) A549 cells (**B**), HepG2/C3A (**C**) cells and HepG3-NTCP cells (**D**) were pre-treated with Indisulam or same amounts of DMSO as control for 48 h, and subsequently infected with Luc-RVFV (MOI= 0.01) for 24 h (**B**), HEV (MOI= 4) (**C**) or HDV (MOI=4) (**D**) for 5 days, respectively. *IFIT1* mRNA (left) and viral mRNA (right) were measured by qPCR. mRNA fold change was normalized on *GAPDH*. Data are derived from three biological replicates (n = 3), error bars refer to SD. Statistical significance was assessed through Welsch's unpaired *t*-test.

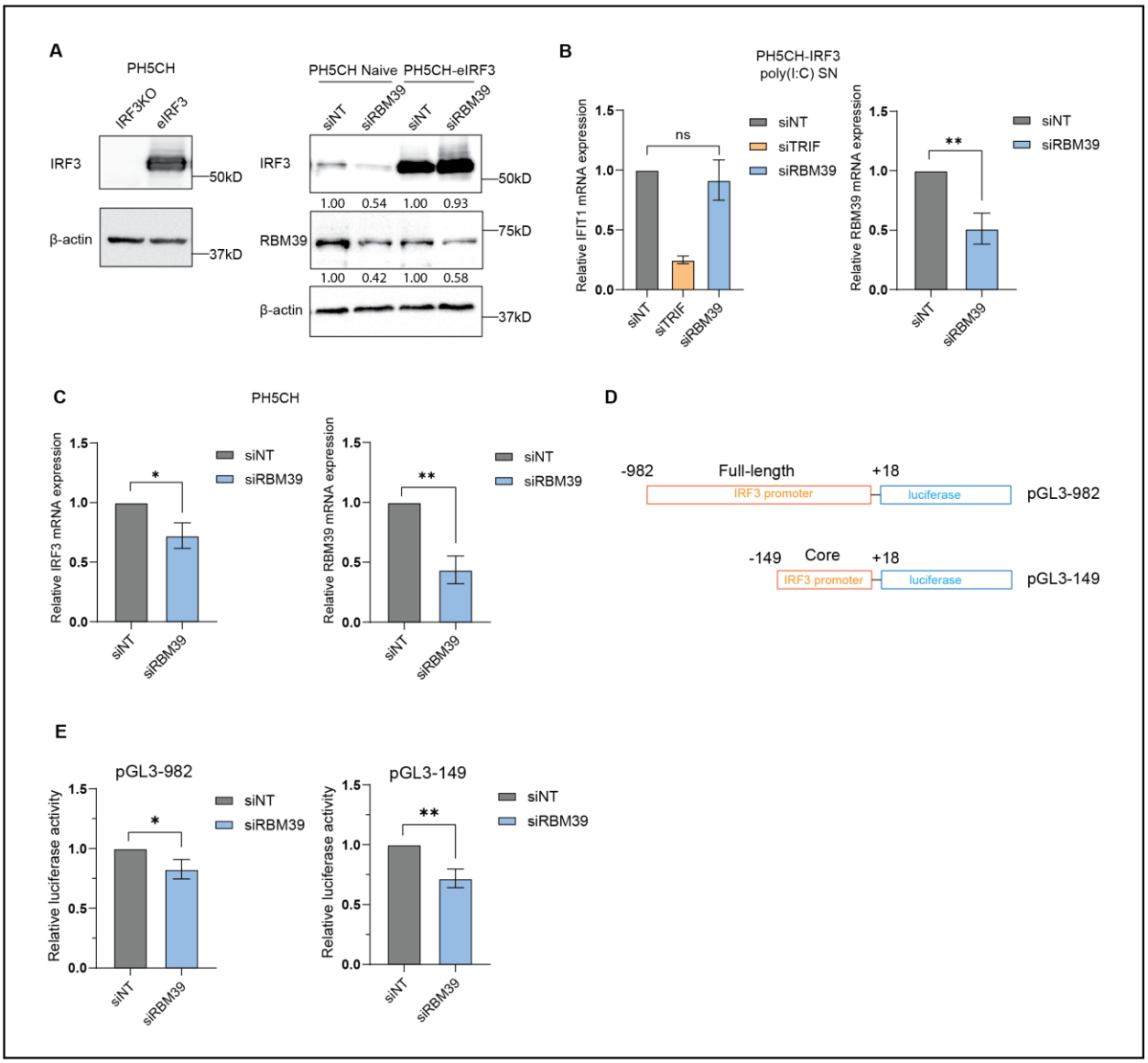


**Fig. 5. RBM39 regulates *IRF3* expression on mRNA level.**

(**A**) Ectopic expression of IRF3 in PH5CH IRF3 KO cells (PH5CH-eIRF3) was determined by western blot (left). PH5CH Naïve or PH5CH-eIRF3 cells, were transfected with siRBM39 or siNT as control for 48 h, IRF3, RBM39 and β-actin were measured by western blot (right). (**B**) PH5CH-eIRF3 cells were transfected with siRBM39 or siNT/siTRIF as controls for 48 h and then fed with 50 μg/ml poly (I:C) in the supernatant for 6 h. *IFIT1* and *RBM39* mRNA expression levels were measured by qPCR. (**C**) PH5CH cells were transfected with siRBM39 or siNT as controls. 48 h after transfection, *IRF3* and *RBM39* mRNA was measured by qPCR. (**D**) Schematic of the firefly luciferase reporter harboring the full-length IRF3 promoter (pGL3-982-firefly) or core IRF3 promoter (pGL3-149-firefly). (**E**) PH5CH cells were transfected with pGL3-982-firefly or pGL3-149-firefly, pGL3-CMV-Gaussia was used as reference. Luciferase activity of firefly was normalized on that of Gaussia. Relative luciferase activity (Relative Light

Units, RLU) is shown. Data indicated are from three biological replicates (n = 3), error bars mean SD. Statistical significance was assessed through Welsch's unpaired *t*-test.

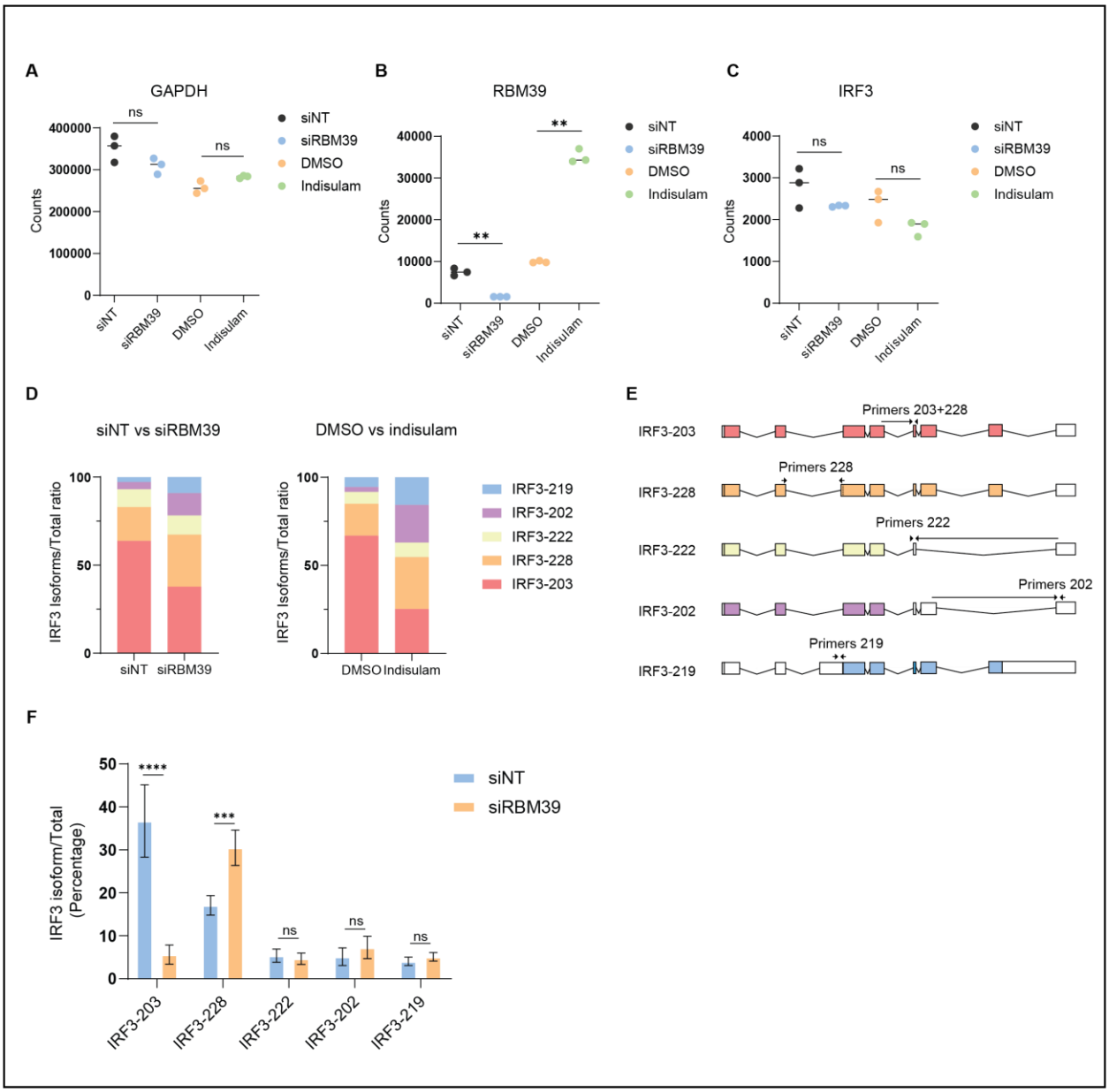


**Fig. 6. Splicing events analysis reveals an IRF3 isoform switch.**

(**A** to **C**) DEG analysis of siRBM39- or Indisulam-treated PH5CH samples. *GAPDH* (**A**), *RBM39* (**B**) and *IRF3* (**C**) mRNA counts were measured by the differential analysis of count data with DESeq2. (**D**) DTU analysis of *IRF3* was performed using DRIMseq. Shown are isoforms/total ratio changes in PH5CH treated with siRBM39 or Indisulam. (**E**) Schematic of *IRF3* isoforms. Specific primers targeting different isoforms are shown as arrows. (**F**) *IRF3* isoforms mRNA expression in PH5CH cells transfected with siRBM39 or siNT as control were

identified by qPCR. Data are from three biological replicates (n = 3), error bars mean ± SD. Statistical significance was assessed through Welsch's unpaired *t*-test.

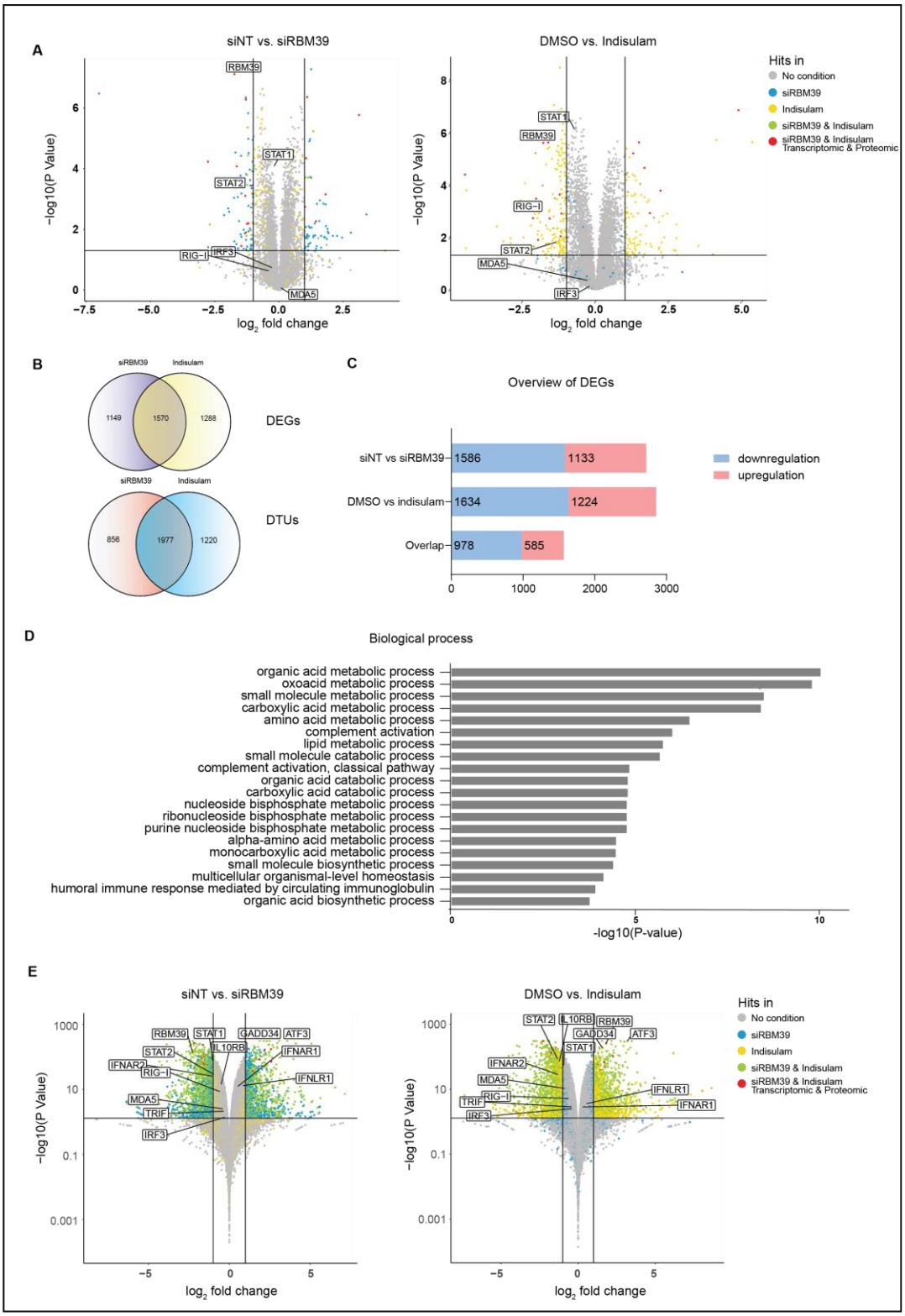

**Fig. 7. Global proteome, transcriptome and splicing analysis.**
(**A**) Volcano plot of proteomic analysis in PH5CH cells treated with siRBM39 vs. siNT (left) or Indisulam vs. DMSO (right) for 48 h. Proteins with fold change > 2 or < -0.5, with p-value < 0.05 in siRBM39 vs. siNT condition (blue), Indisulam vs. DMSO condition (yellow), both conditions (green) in proteomic analysis and hits in both conditions in transcriptomic and proteomics analysis (red) are highlighted. (**B**-**E**) Transcriptomic and splicing analysis of siRBM39 vs. siNT and Indisulam vs. DMSO-treated PH5CH cells. (**B**) Overview of DEG and DTU analysis. DEG and DTU numbers in each condition and overlap are indicated. (**C**) Overview of upregulated and downregulated DEGs. (**D**) Top 20 significantly enriched GO terms for biological processes based on the overlapping DEGs of siRBM39 and Indisulam. (**E**) Volcano plot of DEG analysis in siRBM39 vs. siNT (left) and Indisulam vs. DMSO (right), with DEGs defined as genes with a fold change >2 or <0.5 and a p value <0.05. Hits in only siRBM39 vs. siNT condition (blue), only Indisulam vs. DMSO condition (yellow), both conditions (green) and hits in both conditions in transcriptomic and proteomic analysis (red) are highlighted.

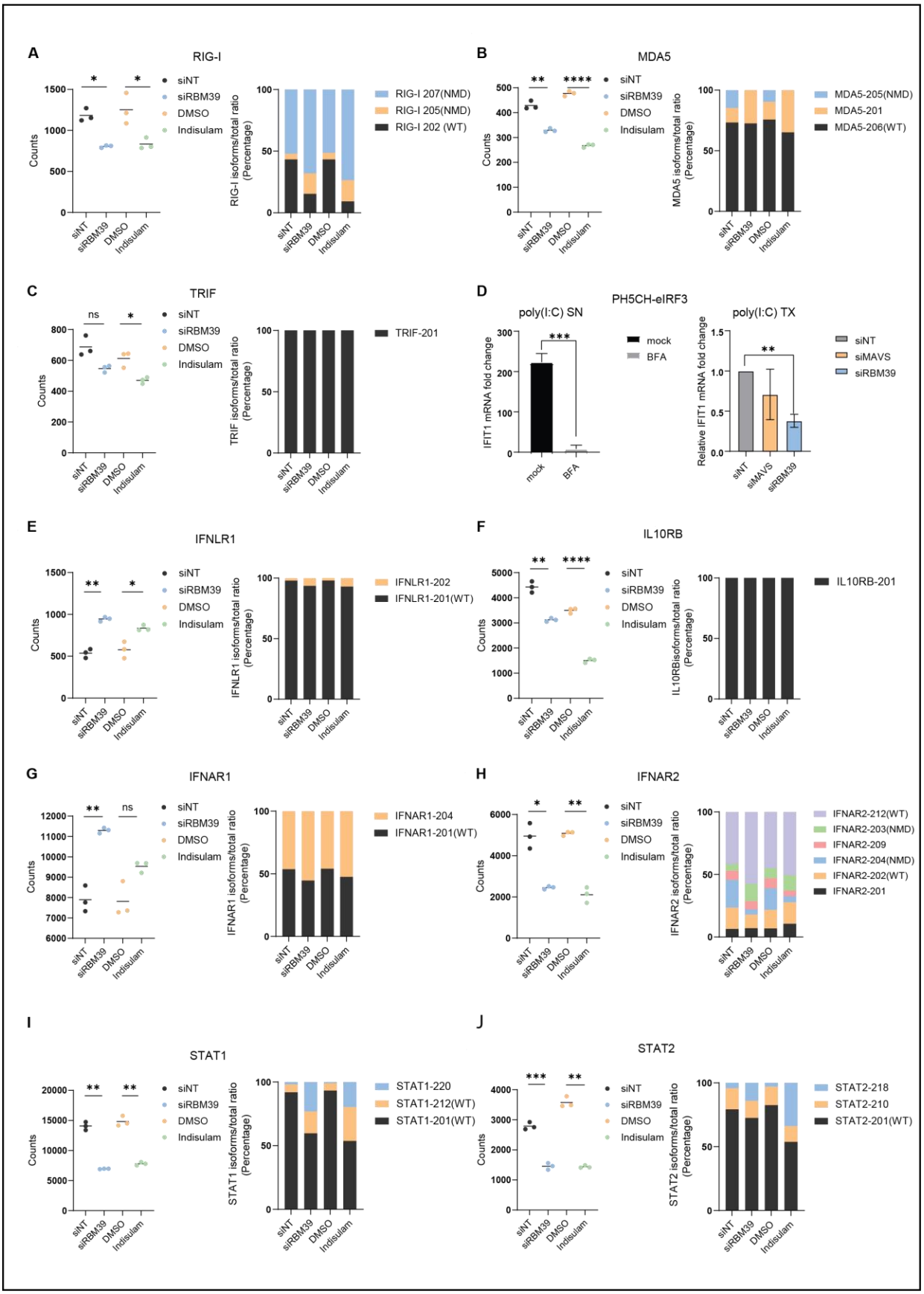
A
RIG-I
Counts
siNT
siRBM39
DMSO
Indisulam
RIG-I isoforms/total ratio (Percentage)
RIG-I 207(NMD)
RIG-I 205(NMD)
RIG-I 202 (WT)
B
MDA5
MDA5 isoforms/total ratio (Percentage)
MDA5-205(NMD)
MDA5-201
MDA5-206(WT)
C
TRIF
TRIF isoforms/total ratio (Percentage)
TRIF-201
D
PH5CH-eIRF3
poly(I:C) SN
IFIT1 mRNA fold change
mock
BFA
poly(I:C) TX
Relative IFIT1 mRNA fold change
siMAVS
E
IFNLR1
IFNLR1 isoforms/total ratio (Percentage)
IFNLR1-202
IFNLR1-201(WT)
F
IL10RB
IL10RBisoforms/total ratio (Percentage)
IL10RB-201
G
IFNAR1
IFNAR1 isoforms/total ratio (Percentage)
IFNAR1-204
IFNAR1-201(WT)
H
IFNAR2
IFNAR2 isoforms/total ratio (Percentage)
IFNAR2-212(WT)
IFNAR2-203(NMD)
IFNAR2-209
IFNAR2-204(NMD)
IFNAR2-202(WT)
IFNAR2-201
I
STAT1
STAT1 isoforms/total ratio (Percentage)
STAT1-220
STAT1-212(WT)
STAT1-201(WT)
J
STAT2
STAT2 isoforms/total ratio (Percentage)
STAT2-218
STAT2-210
STAT2-201(WT)

1012

**Fig. 8. Other key innate immune factors in RBM39 regulatory network.**
(**A** to **C**) Transcriptomic and splicing analysis shows *RIG-I* (**A**), *MDA5* (**B**) and *TRIF* (**C**) gene expression (left) and splicing events (right) in siNT/siRBM39 and DMSO/Indisulam-treated PH5CH cells. (**D**) The inhibition of TLR3 pathway (left) and activation of RIG-I/MDA5 pathway (right). PH5CH-IRF3 cells were treated with siRBM39 or siNT/siMAVs as controls. After 48 h, cells were further pretreated with 10 nM BafilomycinA for 45 min and stimulated with 50 μg/ml or 0.5 μg/ml poly(I:C) via supernatant feeding or transfection, respectively for 6 h. *IFIT1* mRNA was measured by qPCR. mRNA fold change was normalized by *GAPDH*. Relative mRNA expression to siNT control was determined. (**E** to **J**) *IFNLR1* (**E**), *IL10RB* (**F**), *IFNAR1* (**G**), *IFNAR2* (**H**), *STAT1* (**I**) and *STAT2* (**J**) gene expression (left) and splicing events (right) in siNT/siRBM39 and DMSO/Indisulam-treated PH5CH cells. Data are from three biological replicates (n = 3). Statistical significance was assessed through Welsch's unpaired *t*-test.

# Supplementary materials

**The PDF file includes:**

Supplementary methods, Fig. S1 to S8

**Other Supplementary Material for this manuscript includes the following:**

Table S1 to S6

## Supplementary Methods

### Primary mouse hepatocytes isolation:

C57BL6/N wild type mice (9-10 weeks, male) were housed in the specific-pathogen free (SPF) barrier at the Interfakultäre Biomedizinische Forschungseinrichtung (IBF) animal facility at Heidelberg University (Germany). Mice are maintained on a standard diet with ad libitum access to food and water under a constant light-dark cycle. Animal experiment was approved by the Regierungspräsidium Karlsruhe (T47/22). Mice were sacrificed, the abdomen was cleaned with ethanol and then opened expose inferior cava vein and portal vein. The inferior cava vein was Cannulated and washed with pre-warmed Liver Perfusion Medium (ThermoFisher, USA) for about 3-4 minutes until the liver became blood free. Afterwards, the liver was perfused with Liver Digest Medium (ThermoFisher, USA) until it was digested. The liver without gallbladder was transferred to a Petri dish. Cold Hepatocyte Wash Medium (ThermoFisher, USA) was added and the organ liberating cells were de-capsuled. Subsequently, the cells were sequentially passed through 100 µm and 70 µm cell strainers into a 50 mL falcon tube and centrifuged at 50g, 4°C for 2 minutes, to separate liver non-parenchymal cells (NPC) that remain in the supernatant. Next, hepatocytes (HC) pellet was washed with Hepatocyte Wash Medium (ThermoFisher, USA) once and re-suspended in William's E Medium, Glutamax Supplement (ThermoFisher, USA) with 4% FBS, 1% pen-strep and seeded $5 \times 10^4$ cells/cm$^2$ in a collagen-coated plate (Collagen I Rat Protein, Tail, ThermoFisher, USA).

### CRISPR/Cas9 knockout clones:

To generate PH5CH IRF3 single knock-out (KO) clones, PH5CH cells were transduced with the lentiCRISPRv2-IRF3 and lentiviral vectors encoding for Cas9 (see "Plasmids"). After puromycin selection, cells were seeded into 96-well plates for screening of stable single clones.

### siRNA transfection:

The used siRNAs were purchased from Horizon Discovery, UK, unless specifically mentioned. siMAVS was purchased from Sigma Aldrich, Germany. For siRNA transfection in a 6-well plate, Cells with 60%-70% confluency were seeded 16 hours prior to the experiment and 1.5 µM siRNA were mixed with 9 µl Lipofectamine RNAiMax (Thermo Fisher Scientific, USA) in OptiMEM according to manufacturer's instructions. After 20 min

incubation at RT, the mixture was added into the medium. Cells were incubated for 48 h and used for further experiments.

**Mass spectrometry (MS)**

PH5CH cells were treated with siRBM39 or Indisulam for 48 h, siNT and DMSO were used as control. Afterwards, cells were harvested and lysed in 300 µl sodium dodecyl sulfate (SDS) lysis buffer (4% SDS, 10 mM DTT, 55 mM IAA, 50 mM Tris/HCl pH 7.5), and heat-inactivated (95°C for 10 min). The samples were sonicated (4°C, 15x 30 sec on and 30 sec off setting) and the protein lysate was precipitated using pre-chilled acetone (−20°C) at a final concentration of 80% acetone (v/v) overnight. Precipitates were pelleted and washed two times with pre-chilled 80% acetone (-20°C). Pellets were air dried at room temperature and resolubilized by adding 40 µl thiourea buffer (6 M urea, 2 M thiourea (U/T) in 10 mM HEPES, pH 8.0). Protein concentration was determined by BCA assay (Pierce) according to the manufacturer's instructions and adjusted to 50µg with thiourea buffer. Lysates were digested overnight (25°C, 16h, 1200 rpm) using LysC (1:50 w/w, enzyme/protein, Wako) and trypsin (1:50 w/w, enzyme/protein, Promega) per replicate. The samples were prepared for C18-stage tipping by adding 1/5 of loading buffer (10% acetonitrile, 3% TFA) to inactivate proteases (TFA) and enhance solubility (ACN) of samples. Peptides were desalted with 3-layer C18 stage tips (3M). Columns were equilibrated with 200 µl methanol (RT, centrifuge 300xg, 4min), washed twice with 200 µl washing buffer (0.5% acetic acid), loaded with the sample, washed twice with 200 µl washing buffer (0.5% acetic acid) and eluted (80% acetonitrile, 0.5% acetic acid). All steps were executed with 500xg at RT. The eluate was evaporated (45°C, vacuum) and resuspended in MS buffer (2% acetonitrile, 0.3% TFA). Peptide concentrations were measured at 280 nm (Nanodrop 2000, Thermo Scientific), and subsequently equalized to 0.25 µg/µl.

Full proteome samples were measured on a Q Exactive HF mass spectrometer (Thermo Fisher Scientific) coupled online to an EASY-nLC 1200 system (Thermo Fisher Scientific). The liquid chromatography setup consisted of a 75 µm x 50 cm analytical column, packed in-house with Reprosil Pur C18-AQ 1.9 µm particles (Dr. Maisch GmbH). Peptides were separated using a 180 min gradient at a flow rate of 300 nl/min, and a binary buffer system consisting of buffer A 0.1 % (v/v) formic acid in water, and buffer B 80 % (v/v) acetonitrile, 0.1 % (v/v) formic acid in water. More in detail: 5–30% (150 min), 30–95% (10 min), wash out at 95% for 5 min, readjustment to 5% in 5 min, and kept at 5% for 10 min. The mass spectrometer was operated in positive ionization mode, the spray voltage was set to 2.5 kV, funnel RF level at 60, and heated capillary at 250 °C. Full scan MS1 spectra were recorded from 300 to 1,650 m/z at 120 k resolution using an automatic gain control (AGC) target value of 3E6 and a max injection time (IT) of 20 msec. The top 15 peptide precursors were selected for higher energy collisional dissociation (HCD) with 27 % normalized collision energy. The precursor isolation window was set to 1.4 m/z with 15 k MS2 resolution, an AGC target value of 1E5 and a max IT of 25 msec. Only precursors with charge state 2 to 6 were selected and the dynamic exclusion was set to 20 sec.

Raw MS data files of the experiments conducted in data dependent acquisition (DDA) mode were processed with MaxQuant (version 2.0.1.0.) using the default settings and label-free quantification (LFQ) (LFQ min ratio count 2, normalization type classic) enabled. Spectra were searched against forward and reverse sequences of the reviewed human proteome including isoforms (Uniprot, Taxon ID 9606), by the built-in Andromeda search engine. The raw data was analyzed using the “match between runs” option. MaxQuant output file was subsequently processed with Perseus (version 1.6.15.0). Reverse proteins, proteins only

identified by site, and the contaminats were preliminarily filtered out. Then intensities were expressed as Log2(x), imputed (replacing missing values from normal distribution, with.0.3; down shift 1.8), and annotation included. Statistical significance evaluated by "two-sample tests" (Student`s T-test with permutation-based FDR 0.05 and 250 number of randomizations).

## Supplementary Figures

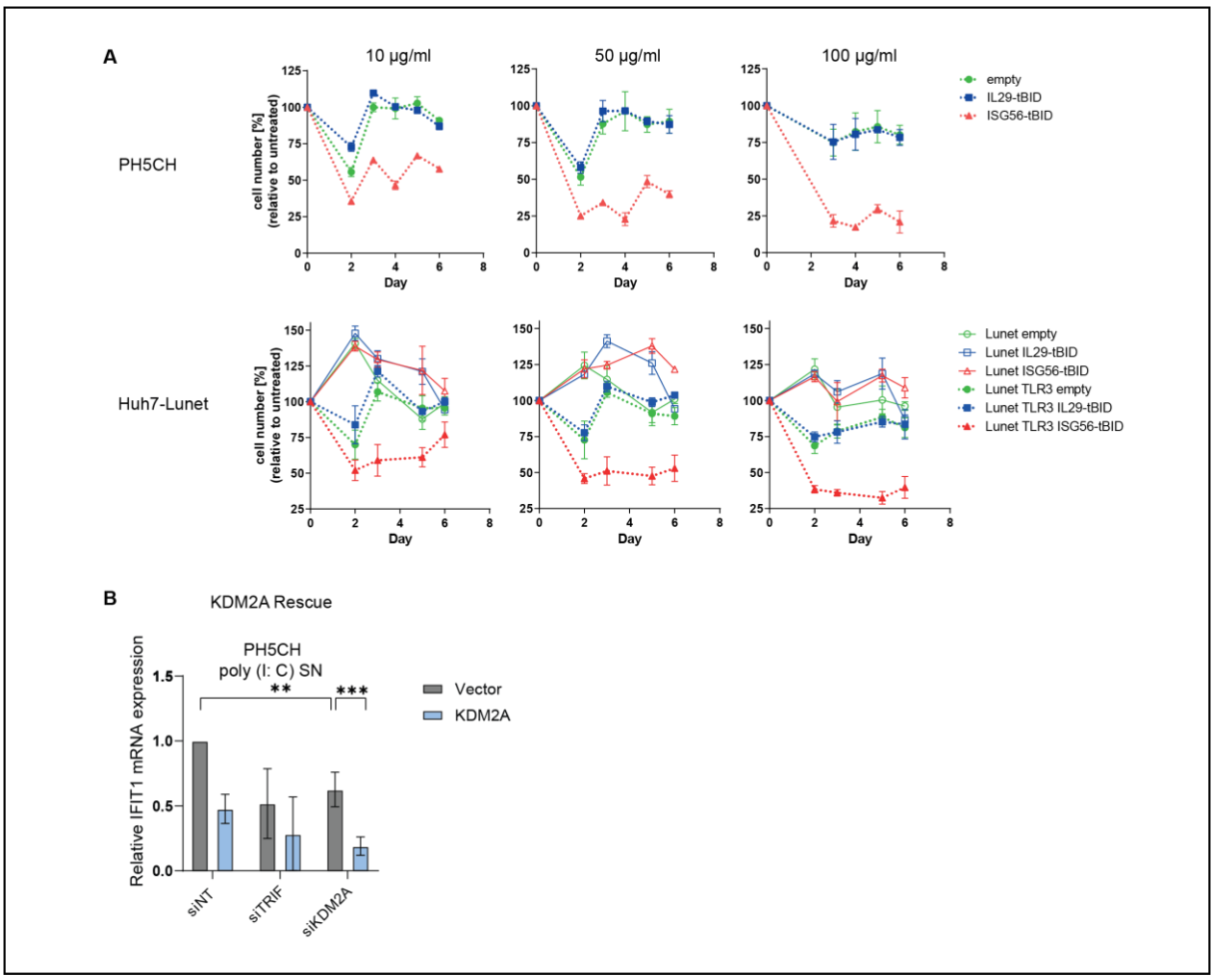


**Fig. S1. Efficiency of the tBID death reporter and rescue of *KDM2A*.**

(**A**) PH5CH cells (upper panel) or Huh7-Lunet cells, with or without ectopic TLR3 (lower panel), stably expressing IFIT1-tBID or empty-tBID death reporter as control were supernatant-fed with the indicated concentrations of poly(I:C), or a same volume of PBS, for the indicated time. Cell viability was determined at the indicated time points using the WST-1 assay. Data are from four independent biological replicates (n=4). (B) Analysis strategy for genome-wide CRISPR/Cas9 screen. Primary sequencing data (green) format was demultiplexed, assigned to different samples and read counts were normalized. The 4 technical replicates (blue for PBS, red for poly(I:C)) of each experiment were averaged. Mean values were used to calculate fold changes for each experiment. Fold changes were thresholded to yield primary hits. After assignment of target gene names, primary hits were filtered by occurrence of multiple sgRNAs per gene and occurrence in multiple datasets to generate a candidate list. (**C**) PH5CH expressing empty vector or *KDM2A* were transfected

with the indicated siRNAs for 48 h. Cells were subsequently stimulated through poly(I:C) supernatant feeding. *IFIT1* mRNA was measured by qPCR. Data are from two biological replicates (n=2), error bars represent SD.

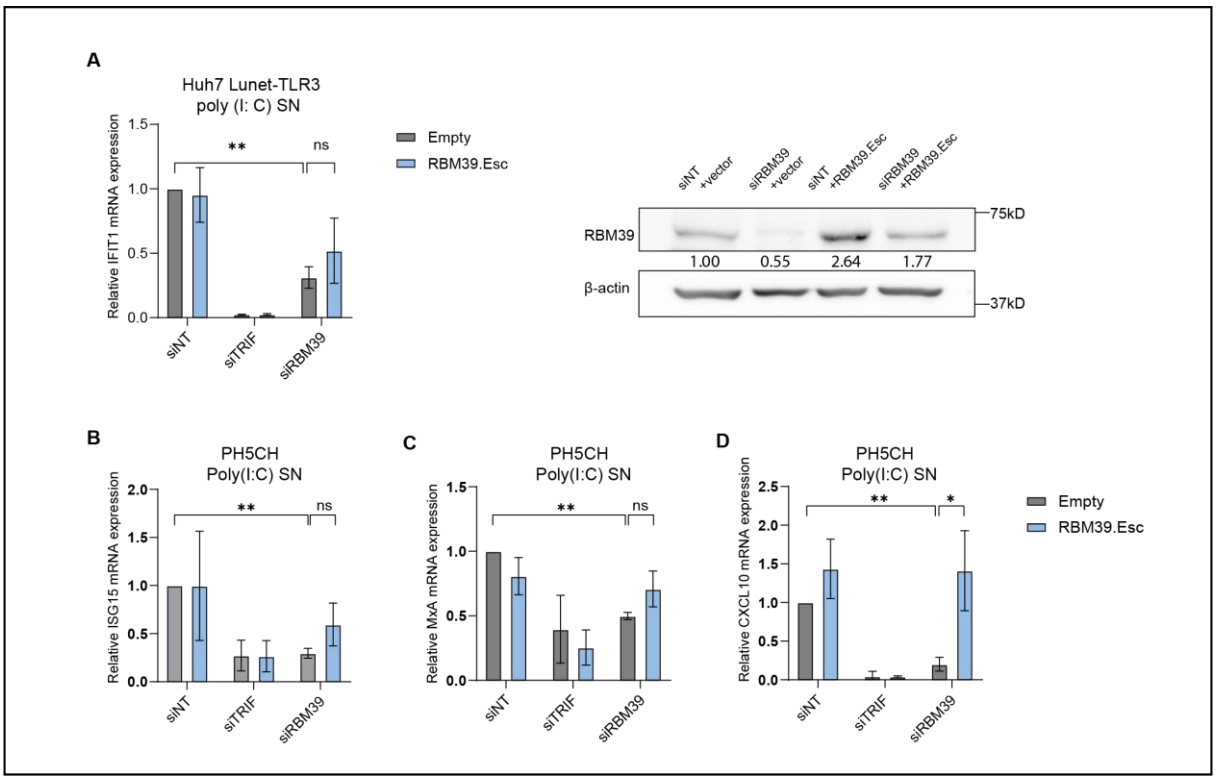


**Fig. S2. RBM39 plays a regulatory function in different cell lines and for multiple ISGs.**

(**A**) Huh7 Lunet-TLR3 cells expressing RBM39.Esc or empty vector were transfected with siRBM39 or siNT/siTRIF as controls for 48 h and then fed with 50 µg/ml poly (I: C) in supernatant for 6 h. *IFIT1* mRNA was measured by qPCR (left), RBM39 expression was measured by western blot (right). (**B** to **D**) PH5CH cells expressing RBM39.Esc or empty vector were treated as above. *ISG15* (**B**), *MxA* (**C**) and *CXCL10* (**D**) mRNA were measured by qPCR. Data are from three biological replicates (n = 3), error bars mean ± SD. Statistical significance was assessed through Welsch's unpaired *t*-test.

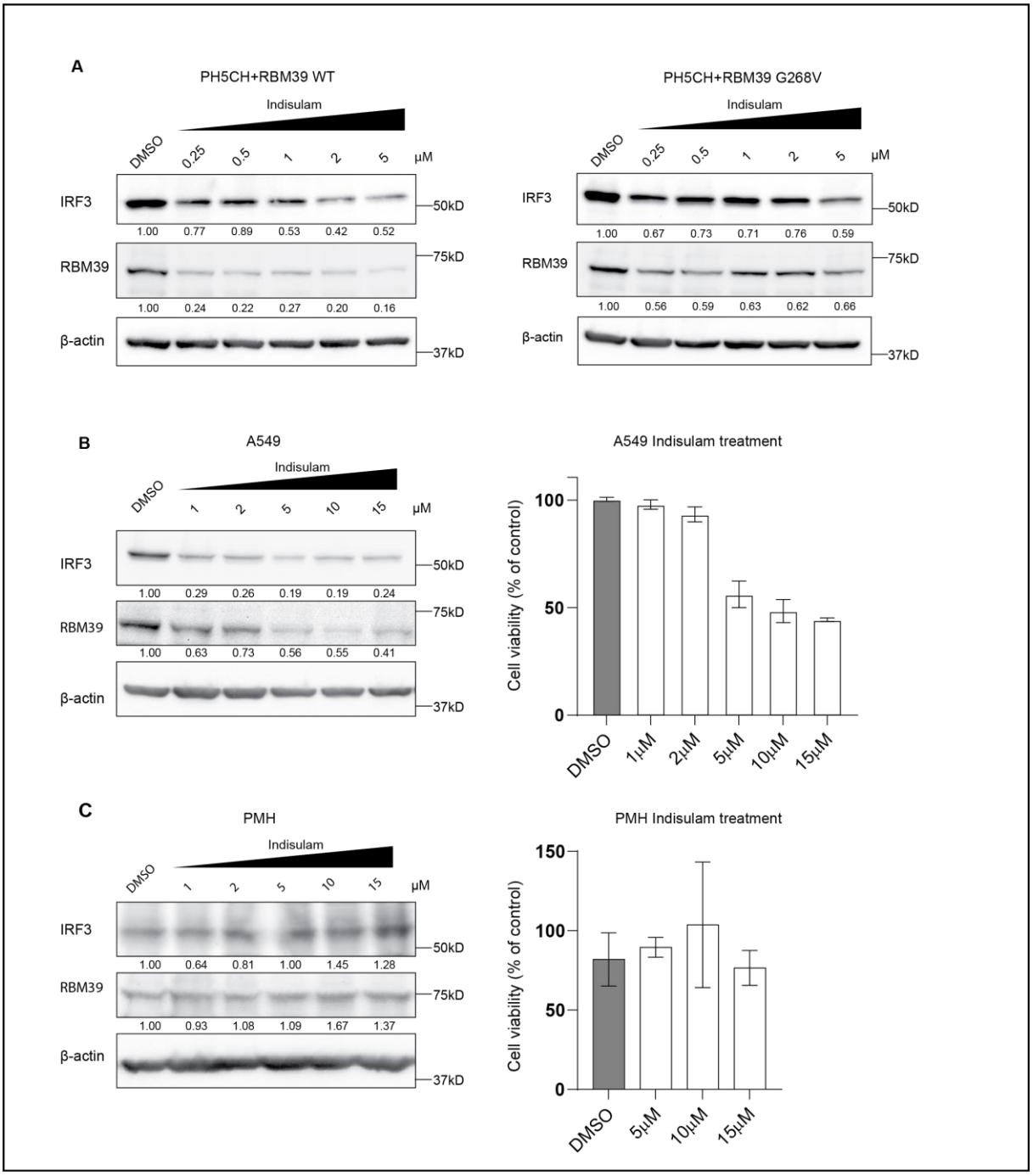


**Fig. S3. Indisulam-mediated degradation of RBM39 affects IRF3 in different cell lines.**

(**A** to **C**) PH5CH-RBM39 and PH5CH-RBM39 G268V cells (**A**), A549 cells (**B**), PMH (**C**) were treated with Indisulam at the indicated concentrations for 48 h. IRF3, RBM39 and β-actin protein expression levels were measured by western blot. Quantification of three independent experiments is shown as average number under the respective bands. (left) Cell viability was measured via CellTiter-Glo luminescent cell viability assay (**B** and **C**, right). Data are from three biological replicates (n = 3), error bars indicate SD.

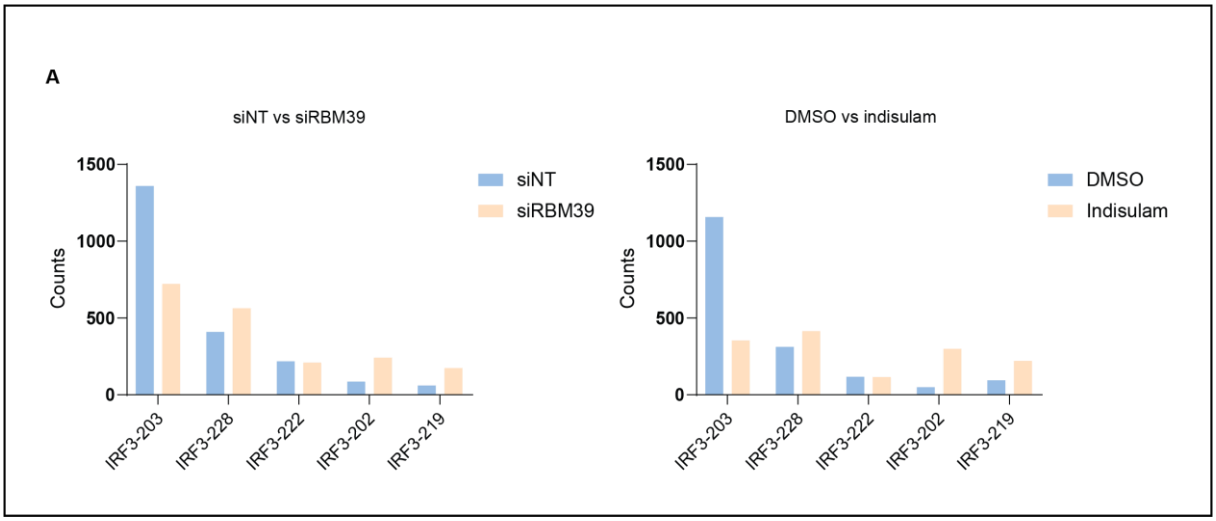


**Fig. S4. Absolute mRNA counts of *IRF3* isoforms upon Indisulam treatment/ siRBM39 knockdown.**

(**A**) DTU analysis of *IRF3* isoforms in PH5CH cells treated with siRBM39 vs. siNT (left) or Indisulam vs. DMSO (right) was performed using DRIMseq. Shown is the absolute mRNA count of *IRF3* isoforms. Data are derived from three biological replicates (n = 3).

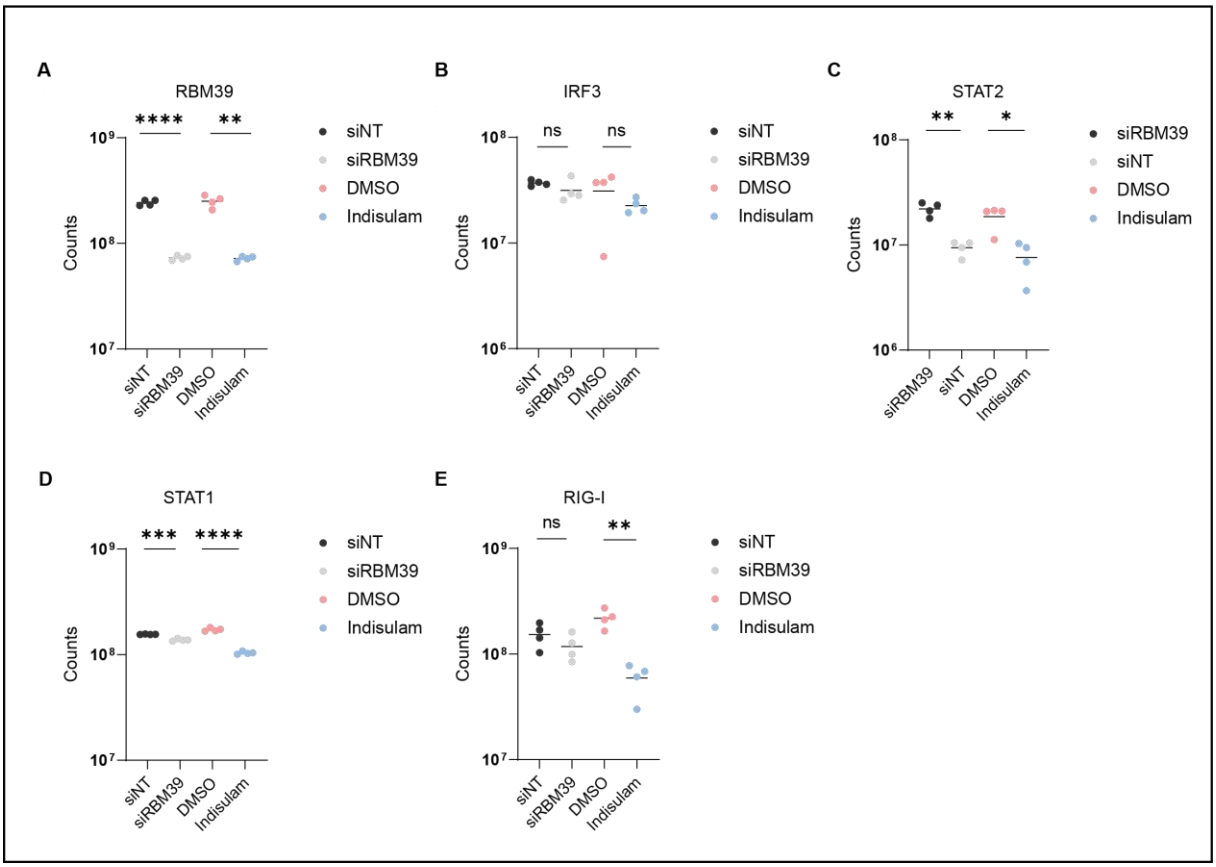


**Fig. S5. Protein expression of several key innate immune factors upon Indisulam treatment/ siRBM39 knockdown.**

(**A** to **E**) Proteomic analysis shows RBM39 (**A**), STAT1 (**B**), STAT2 (**C**), RIG-I (**D**) and IRF3 (**E**) protein expression in PH5CH cells treated with siRBM39 vs. siNT or Indisulam vs. DMSO. Data are from four biological replicates (n = 4). Statistical significance was assessed through Welsch's unpaired *t*-test.

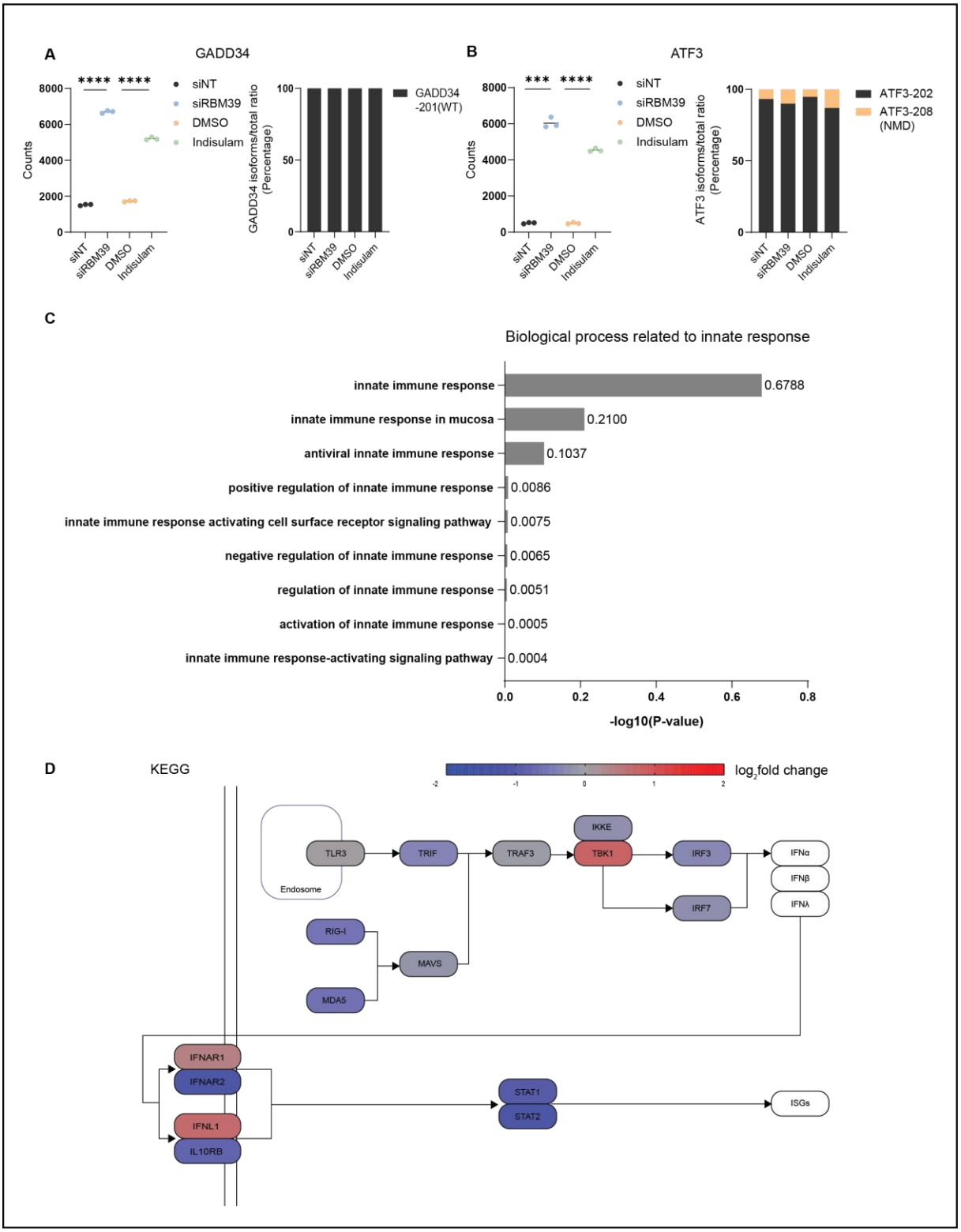


**Fig. S6. Transcriptomic and splicing analysis of relevant innate immune pathways.**

(**A** to **B**) Transcriptomic and splicing analyses show *GADD34* (**A**) and *ATF3* (**B**) gene expression (left) and splicing events (right) in PH5CH cells treated with siRBM39 vs. siNT, or Indisulam vs. DMSO. (**C**) Enrichment analysis for GO terms related to innate immune pathways based on the overlapping DEGs of siRBM39 and Indisulam. (**D**) Enrichment analysis for GO terms related to innate immunity based on the overlapping DEGs of siRBM39 and Indisulam-treated samples.